이학박사 학위논문

Nonconforming Finite Element Methods for Stokes and Elliptic Problems

스토크스 문제와 타원형 편미분 방정식에 대한 비순응 유한요소법

2014 년 2 월

서울대학교 대학원

수리과학부

심 광 신

이학박사 학위논문

Nonconforming Finite Element Methods for Stokes and Elliptic Problems

스토크스 문제와 타원형 편미분 방정식에 대한 비순응 유한요소법

2014 년 2 월

서울대학교 대학원

수리과학부

심 광 신

Nonconforming Finite Element Methods for Stokes and Elliptic Problems

스토크스 문제와 타원형 편미분 방정식에 대한 비순응 유한요소법

지도교수 신 동 우

이 논문을 이학박사 학위논문으로 제출함

2013 년 10 월

서울대학교 대학원

수리과학부

심 광 신

심 광 신의 이학박사 학위논문을 인준함

2013 년 12 월

위 원 장	정 상 권	(인)
부위원장	신 동 우	(인)
위 원	전 영 목	(인)
위 원	박 춘 재	(인)
위 원	남 현	(인)

Abstract

Nonconforming Finite Element Methods for Stokes and Elliptic Problems

Kwangshin Shim
Department of Mathematical Sciences
The Graduate School
Seoul National University

A new class of nonparametric nonconforming quadrilateral finite elements is introduced in Chapter 1, which has the midpoint continuity and the mean value continuity at the interfaces of elements simultaneously as the rectangular DSSY element [8]. The parametric DSSY element for general quadrilaterals requires five degrees of freedom to have an optimal order of convergence [4], while the new nonparametric DSSY elements require only four degrees of freedom. The design of new elements is based on the decomposition of a bilinear transform into a simple bilinear map followed by a suitable affine map. Numerical results are presented to compare the new elements with the parametric DSSY element.

In Chapter 2, as in two dimension, a class of nonparametric DSSY element in three dimensional hexahedral mesh is designed. It satisfies the optimal convergence property in genuine hexahedral mesh (consisting of six flat faces) with six local basis functions contrast to the parametric DSSY element. Also, the case of hexahedron mesh with non-flat faces is discussed. The numerical results for the genuine hexahedral mesh and the non-flat hexahedral mesh are presented.

A new nonparametric nonconforming quadrilateral finite element is introduced in Chapter 3. The finite element is based on the nonparametric DSSY element introduced in Chapter 1 and constructed to have the minimal value of H^1-seminorm on each element as in [11]. From this, the finite element has the maximal inf-sup constant and performs better than the nonparametric DSSY element introduced in Chapter 1 in the aspect of computing time. Numerical results are presented to show the speedup of computation by comparing with [13].

Keywords : nonconforming finite element, DSSY finite element, nonparametric finite element, the incompressible Stokes equations, the elliptic problem, the planar linear elasticity problem

Student Number : 2010-30086

Contents

List of Figures

List of Tables

Chapter 1

Two-dimensional nonparametric DSSY elements

1.1 Introduction

There have been many progresses for nonconforming finite element methods for many mechanical problems for last decades. Nonconforming elements have been a favorite choice in solving the Stokes and Navier-Stokes equations [5, 7, 19, 22, 25] in a stable manner. Also, the nonconforming nature facilitates resolving numerical locking [3, 16, 27] in elasticity problems with the clamped boundary condition. For pure traction boundary value problems in elasticity, there have been a couple of approaches to avoid numerical locking by employing conforming and nonconforming elements componentwise [15, 17, 18]. Although there are several higher-order nonconforming elements, the lowest order nonconforming elements have been especially popular numerical methods because of its simplicity and stability property [7, 22, 25]. In particular, the

linear simplicial nonconforming elements introduced by Crouzeix and Raviart [7] have been most widely used. Since the degrees of freedom for quadrilateral or rectangular elements are usually smaller than those for triangular elements, it is desirable to use quadrilateral or rectangular elements wherever they can be applied.

We briefly review some progresses for nonconforming rectangular or quadrilateral elements. Han introduced firstly a rectangular element which assumes five local degrees of freedom (DOFs) [9] in 1984. Then in 1992 Rannacher and Turek introduced the rotated Q_1 nonconforming elements with two types of degrees of freedom [22]: the four edge-midpoint value DOFs and the four edge integral DOFs. Chen [6] also used the first type of DOFs for the same rotated Q_1 element. Douglas, Santos, Sheen and Ye introduced a new nonconforming finite element, which we call the *DSSY element* in this paper, for which the two types of degrees of freedom are coincident on rectangular (or parallelogram) meshes [8]. One of the key features of this DSSY element is that it fulfills the *mean value property* on each edge. For a convergence analysis, the average continuity property over each edge implies the pass of "patch test", which is a sufficient condition for optimal convergence of nonconforming finite element methods [23, 24, 26]. Notice that using the edge-midpoint values is not only cheaper but also simpler than using edge-integral values in constructing the local and global basis functions. For instance, in gluing two neighboring elements across an edge, only one evaluation at the edge midpoint is necessary for the DSSY-type element while at least two Gauss-point evaluations are necessary for the elements using integral type DOFs. Therefore, nonconforming elements fulfilling the mean value property have advantages in implementation. The Crouzeix-Raviart P_1-nonconforming elements [7] enjoy the mean value property.

Arnold, Boffi, and Falk provided a theory of convergence order in quadrilateral meshes [1]. A modified DSSY element was introduced in [4], which requires an additional DOF in order to retain an optimal convergence order for genuinely quadrilateral meshes. It seems impossible to reduce the number of DOFs from five to four as long as one considers a parametric DSSY-type element on quadrilateral meshes and still wants to preserve optimal convergence.

The aim of this paper is to attempt to extend the spirit of rectangular DSSY element to genuinely quadrilateral meshes keeping the mean value property with four DOFs, shifting from the parametric realm to the nonparametric one. Our starting point is based on a clever decomposition of a bilinear map into a simple bilinear map followed by an affine map [14, 20, 21]. This approach induces an intermediate reference quadrilateral, where a four DOF DSSY-type element can be defined. Then the affine map will preserve P_1 and the mean value property on each edge. We remark that the quadrilateral element introduced in [20] is of only three DOFs, and a similar element was introduced by Hu and Shi [10], but without any modification they cannot be used to solve fluid and solid mechanics in a stable manner.

The paper is organized as follows. In section 2 we review some specific properties of the DSSY element. Then using the decomposition of a bilinear map into a simple bilinear map followed by an affine map, we introduce a family of quadrilateral elements on an intermediate reference quadrilateral, which is of four DOFs. Based on this, we define a family of nonparametric quadrilateral elements. Section 3 is devoted to numerical experiments. The performance of the new nonparametric DSSY elements and the parametric DSSY element is compared in terms of computation time where the nonparametric DSSY elements show a clear advantage over the parametric one.

1.2 Quadrilateral nonconforming elements

In this section we will introduce a nonparametric DSSY element of four local degrees of freedom. First of all let us review the (parametric) DSSY element in brief.

1.2.1 The DSSY element

Let Ω be a simply connected polygonal domain in $\mathbb{R}^2$ and $(\mathcal{T}_h)_{h>0}$ be a family of shape regular quadrilateral triangulations of Ω with $\max_{K\in\mathcal{T}_h} \mathrm{diam}(K) = h$. Let us denote by $\mathcal{E}_h$ the set of all edges in $\mathcal{T}_h$. For an element $K \in \mathcal{T}_h$ we denote four vertices of K by $\mathbf{v}_j$ for $j = 1, 2, 3, 4$. Also denote the edge passing through $\mathbf{v}_{j-1}$ and $\mathbf{v}_j$ by e_j and the midpoint of e_j by $\mathbf{m}_j$ for $j = 1, 2, 3, 4$, (assuming $\mathbf{v}_0 := \mathbf{v}_4$,) as in Figure 1.1. The linear polynomials l_{13} and l_{24} are defined in a way that two line equations $l_{13} = 0$, $l_{24} = 0$ pass through $\mathbf{m}_1$, $\mathbf{m}_3$, and $\mathbf{m}_2$, $\mathbf{m}_4$, respectively. Consider a reference square $\widehat{K} = [-1, 1]^2$. We use the similar notations for vertices, edges, midpoints of $\widehat{K}$ as those of K such as $\widehat{\mathbf{v}}_j$, $\widehat{e}_j$, and $\widehat{\mathbf{m}}_j$ for $j = 1, 2, 3, 4$.

Let $K \in \mathcal{T}_h$ be any quadrilateral. Then there exists a bilinear map $\mathcal{F}_K : \widehat{K} \to K$ such that $\mathcal{F}_K(\widehat{K}) = K$. Notice that $\mathcal{F}_K$ can be written as follows:

$$\mathcal{F}_K(\widehat{\mathbf{x}}) = \mathbf{v}_1 + \frac{1-\widehat{x}_1}{2}(\mathbf{v}_2 - \mathbf{v}_1) + \frac{1-\widehat{x}_2}{2}(\mathbf{v}_4 - \mathbf{v}_1) + \frac{(1-\widehat{x}_1)(1-\widehat{x}_2)}{4}(\mathbf{v}_1 - \mathbf{v}_2 + \mathbf{v}_3 - \mathbf{v}_4). \tag{1.1}$$

Set

$$\mathcal{NC}^{DSSY}_{\widehat{K},l} = \{1, \widehat{x}_1, \widehat{x}_2, \widehat{\varphi}_l(\widehat{x}_1) - \widehat{\varphi}_l(\widehat{x}_2)\}, \quad l = 1, 2,$$

where

$$\widehat{\varphi}_l(t) = \begin{cases} t^2 - \frac{5}{3}t^4, & l = 1, \\ \\ t^2 - \frac{25}{6}t^4 + \frac{7}{2}t^6, & l = 2. \end{cases} \tag{1.2}$$

Then the degrees of freedom for the DSSY element can be chosen as either four mean values over edges or four edge-midpoint values, which turn out to be identical. In other words, the DSSY elements fulfill the *mean value property*:

$$\frac{1}{|\widehat{e}_j|}\int_{\widehat{e}_j} \widehat{v}\; d\widehat{\sigma} = \widehat{v}(\widehat{\mathbf{m}}_j), \qquad j=1,2,3,4, \quad \forall \widehat{v} \in \mathcal{NC}^{DSSY}_{\widehat{K},l}. \tag{1.3}$$

In order to retain an optimal convergence order for any quadrilateral mesh, the parametric DSSY element needs an additional element $\widehat{x}_1\widehat{x}_2$, and therefore the modified reference element reads

$$\mathcal{NC}^{DSSY^*}_{\widehat{K},l} = \{1, \widehat{x}_1, \widehat{x}_2, \widehat{x}_1\widehat{x}_2, \widehat{\varphi}_l(\widehat{x}_1) - \widehat{\varphi}_l(\widehat{x}_2)\}, \quad l=1,2,$$

with an additional degree of freedom

$$\int_{\widehat{K}} \widehat{v}(\widehat{\mathbf{x}})\widehat{x}_1\widehat{x}_2 \;\; \mathrm{d}\widehat{\mathrm{x}}_1\mathrm{d}\widehat{\mathrm{x}}_2\,.$$

The DSSY element on K is then defined by

$$\mathcal{NC}^{DSSY}_K = \begin{cases} \{v \mid v = \widehat{v}\circ\mathcal{F}_K^{-1}, \widehat{v} \in \mathcal{NC}^{DSSY^*}_{\widehat{K},l}\} & \text{if } K \text{ is a true quadrilateral,} \\ \{v \mid v = \widehat{v}\circ\mathcal{F}_K^{-1}, \widehat{v} \in \mathcal{NC}^{DSSY}_{\widehat{K},l}\} & \text{if } K \text{ is a rectangle,} \end{cases}$$

where $\mathcal{F}_K$ is defined by (1.1). The global parametric DSSY element is defined by

$$\begin{aligned} \mathcal{NC}^p_h = \{v_h \in L^2(\Omega) \mid v_h|_K \in \mathcal{NC}^{DSSY}_K \text{ for } K \in \mathcal{T}_h, v_h \text{ is} \\ \text{continuous at the midpoint of each } e \in \mathcal{E}_h\}, \\ \mathcal{NC}^p_{h,0} = \{v_h \in \mathcal{NC}^p_h \mid v_h \text{ is zero at the midpoint of } e \in \mathcal{E}_h \cap \partial\Omega\}. \end{aligned}$$

1.2.2 A Class of Nonparametric DSSY Elements

We are interested in reducing the five degrees of freedom DSSY element to four, but still retaining the *mean value property* (1.3). It seems that there does not exist a four-DOF parametric quadrilateral element which has an optimal order convergence rate and the *mean value property* simultaneously. Here, we seek a candidate among nonparametric elements.

A closer look at the DSSY element

For the sake of simplicity of our argument regrading the geometrical property of a basis function, we shall focus on, $\widehat{\varphi}_1(\widehat{x}_1) - \widehat{\varphi}_1(\widehat{x}_2)$.

Let us denote $\widehat{\varphi}_1(\widehat{x}_1) - \widehat{\varphi}_1(\widehat{x}_2)$ by $\widehat{\psi}(\widehat{\mathbf{x}})$ for convenience. In the reference domain $\widehat{K}$, the function $\widehat{\psi}(\widehat{\mathbf{x}})$ can be factorized as

$$\widehat{\psi}(\widehat{\mathbf{x}}) = -\frac{5}{3}(\widehat{x}_1 - \widehat{x}_2)(\widehat{x}_1 + \widehat{x}_2)(\widehat{x}_1^2 + \widehat{x}_2^2 - \frac{3}{5}), \tag{1.4}$$

from which one can realize that $\widehat{\psi}(\widehat{\mathbf{x}})$ is the product of three polynomials whose zero-level sets consist of the two diagonals of $\widehat{K}$ and one circle $\widehat{x}_1^2 + \widehat{x}_2^2 - \frac{3}{5} = 0$ in $\widehat{K}$. At this point, a natural question is whether for any quadrilateral K we may find a function satisfying the *mean value properties* by using the similar geometrical idea as $\widehat{\psi}(\widehat{\mathbf{x}})$.

Among the parametric nonconforming elements in [8], $\psi(\mathbf{x}) = \widehat{\psi} \circ \mathcal{F}_K^{-1}$ is not a quartic polynomial in general if K is a genuine quadrilateral, that is, if $\mathcal{F}_K$ is not an affine map. In most cases it is a non-polynomial function. Thus $\psi(\mathbf{x})$ would not be similarly regarded as the product of zero level set functions of three geometrical objects, such as two lines and a circle. This seems to be one of the limits of using parametric elements. We will thus divert our attention from using the parametric elements and investigate a possible

way of finding a suitable four degrees of freedom element.

Intermediate Spaces

To design such a suitable element, we first decompose the bilinear map $\mathcal{F}_K$ given by (1.1) into a composition of a *simple bilinear map* followed by an affine map [14, 20, 21]. A bilinear map $S : \mathbb{R}^2 \to \mathbb{R}^2$ is said to be a *simple bilinear map* if there exists a vector $\widetilde{\mathbf{s}}$ such that $S\binom{x_1}{x_2} = \binom{x_1}{x_2} + x_1 x_2 \widetilde{\mathbf{s}}$ for all $\binom{x_1}{x_2} \in \mathbb{R}^2$.

Observe that $\mathcal{F}_K$ can be written as follows:

$$\mathcal{F}_K(\widehat{\mathbf{x}}) = A\widehat{\mathbf{x}} + \widehat{x}_1\widehat{x}_2\mathbf{d} + \mathbf{b} = A\left[\widehat{\mathbf{x}} + \widehat{x}_1\widehat{x}_2 A^{-1}\mathbf{d}\right] + \mathbf{b} = A\left[\widehat{\mathbf{x}} + \widehat{x}_1\widehat{x}_2\widetilde{\mathbf{s}}\right] + \mathbf{b}, \qquad (1.5)$$

where A is a 2×2 matrix and $\mathbf{b}, \mathbf{d}$, and $\widetilde{\mathbf{s}}$ are two-dimensional vectors given by

$$\begin{aligned} A &= \frac{1}{4}\left(\mathbf{v}_1 - \mathbf{v}_2 - \mathbf{v}_3 + \mathbf{v}_4, \mathbf{v}_1 + \mathbf{v}_2 - \mathbf{v}_3 - \mathbf{v}_4\right), \\ \mathbf{d} &= \frac{\mathbf{v}_1 - \mathbf{v}_2 + \mathbf{v}_3 - \mathbf{v}_4}{4}, \quad \mathbf{b} = \frac{\mathbf{v}_1 + \mathbf{v}_2 + \mathbf{v}_3 + \mathbf{v}_4}{4}, \quad \widetilde{\mathbf{s}} = A^{-1}\mathbf{d}. \end{aligned}$$

Notice that (1.5) can be understood as the following decomposition of an affine map and a *simple bilinear map* associated with $\widetilde{\mathbf{s}}$:

$$\mathcal{F}_K = \mathcal{A}_K \circ \mathcal{S}_K,$$

where $\mathcal{A}_K : \widetilde{K} \to K$ and $\mathcal{S}_K : \widehat{K} \to \widetilde{K}$ are given by

$$\mathcal{A}_K(\widetilde{\mathbf{x}}) = A\widetilde{\mathbf{x}} + \mathbf{b}, \quad \mathcal{S}_K(\widehat{\mathbf{x}}) = \widehat{\mathbf{x}} + \widehat{x}_1\widehat{x}_2\widetilde{\mathbf{s}}.$$

Here, $\widetilde{K} = \mathcal{S}_K(\widehat{K})$ is a quadrilateral with four vertices

$$\widetilde{\mathbf{v}}_1 = \widehat{\mathbf{v}}_1 + \widetilde{\mathbf{s}}, \quad \widetilde{\mathbf{v}}_2 = \widehat{\mathbf{v}}_2 - \widetilde{\mathbf{s}}, \quad \widetilde{\mathbf{v}}_3 = \widehat{\mathbf{v}}_3 + \widetilde{\mathbf{s}}, \quad \widetilde{\mathbf{v}}_4 = \widehat{\mathbf{v}}_4 - \widetilde{\mathbf{s}}.$$

It should be stressed that the midpoints of $\widehat{K}$ are invariant under the map $\mathcal{S}_K$ and that $\widetilde{K}$ is a perturbation of $\widehat{K}$ by a single vector $\widetilde{\mathbf{s}}$ such that opposite vertices are moved in the same direction (see Figure 1.1).

The relations of three mappings $\mathcal{A}_K, \mathcal{S}_K, \mathcal{F}_K$ and three domains $\widehat{K}, \widetilde{K}, K$ can be interpreted as follows. For given quadrilateral $K \in \mathcal{T}_h$ and the reference cube $\widehat{K}$, $\mathcal{F}_K$ is a unique bilinear map such that $\mathcal{F}_K(\widehat{\mathbf{v}}_j) = \mathbf{v}_j$ for $j = 1, 2, 3, 4$. It is easy to see that there exists a unique simple bilinear map $\mathcal{S}_K$ and $\widetilde{K}$ such that $\widetilde{K} = \mathcal{S}_K(\widehat{K})$ and $K = \mathcal{A}_K(\widetilde{K})$. The intermediate reference domain $\widetilde{K}$ is very useful when we construct a certain type of basis functions that have specific features in K since $\widetilde{K}$ is connected to the physical domain K by an affine map not by a bilinear map. Adapted to this spirit, we will construct basis functions in $\widetilde{K}$ instead of $\widehat{K}$.

Remark 1.2.1. *Notice that $\widetilde{K}$ is convex if and only if*

$$|\widetilde{s}_1| + |\widetilde{s}_2| \leq 1, \tag{1.6}$$

where the equality holds if and only if $\widetilde{K}$ degenerates to a triangle [21].

Our strategy is to use the intermediate reference domain $\widetilde{K}$, where the ansatz is to set a quartic polynomial similarly to (1.4) as follows:

$$\widetilde{\mu}(\widetilde{\mathbf{x}}) = -\frac{5}{3}\widetilde{\ell}_1(\widetilde{\mathbf{x}})\widetilde{\ell}_2(\widetilde{\mathbf{x}})\widetilde{\mathcal{Q}}(\widetilde{\mathbf{x}}), \tag{1.7}$$

where $\widetilde{\ell}_j(\widetilde{\mathbf{x}}), j = 1, 2$, are linear polynomials and $\widetilde{\mathcal{Q}}(\widetilde{\mathbf{x}})$ a quadratic polynomial. We seek a quartic polynomial $\widetilde{\mu}(\widetilde{\mathbf{x}})$ fulfilling the *mean value property* (1.3) in $\widetilde{K}$. Naturally, set $\widetilde{\ell}_1(\widetilde{\mathbf{x}})$ and $\widetilde{\ell}_2(\widetilde{\mathbf{x}})$ to be linear polynomials such that $\widetilde{\ell}_1(\widetilde{\mathbf{x}}) = 0$ and $\widetilde{\ell}_2(\widetilde{\mathbf{x}}) = 0$ are the equations of lines passing through $\widetilde{\mathbf{v}}_1$, $\widetilde{\mathbf{v}}_3$, and $\widetilde{\mathbf{v}}_2$, $\widetilde{\mathbf{v}}_4$,

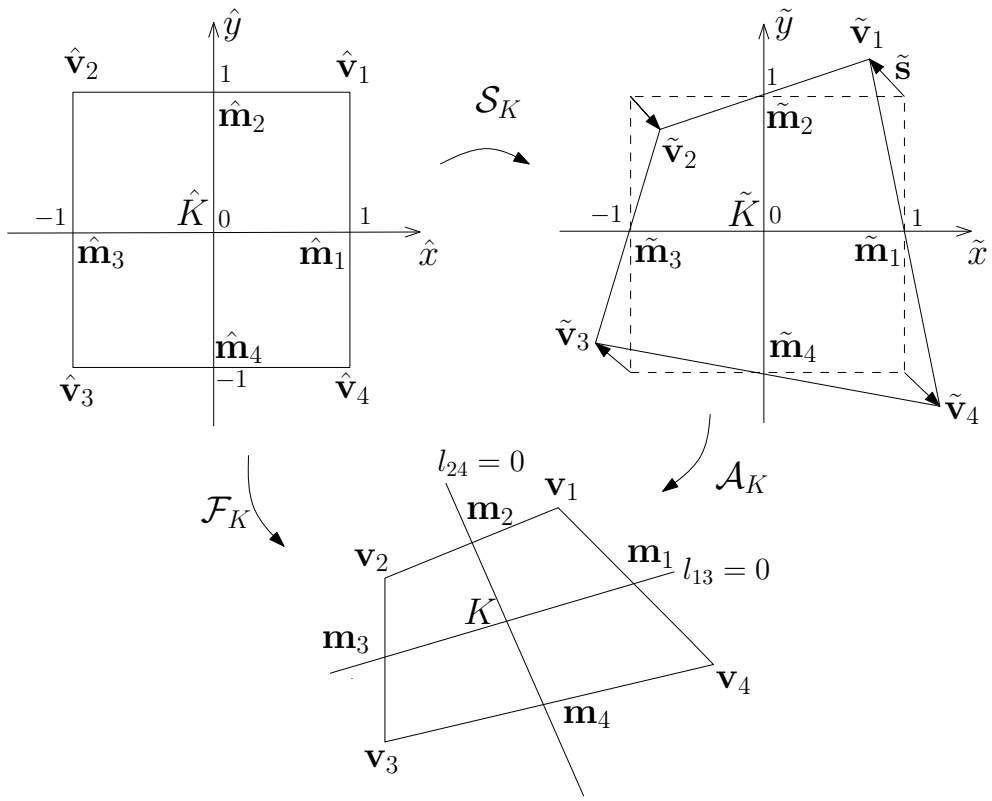

Figure 1.1: A bilinear map $\mathcal{F}_K$ from $\widehat{K}$ to K, a bilinear map $\mathcal{S}_K$ from $\widehat{K}$ to $\widetilde{K}$, and an affine map $\mathcal{A}_K$ from $\widetilde{K}$ to K.

respectively. Then they are given (up to multiplicative constants) by

$$\widetilde{\ell}_1(\widetilde{\mathbf{x}}) = \widetilde{x}_1 - \widetilde{x}_2 + \widetilde{s}_2 - \widetilde{s}_1, \tag{1.8a}$$

$$\widetilde{\ell}_2(\widetilde{\mathbf{x}}) = \widetilde{x}_1 + \widetilde{x}_2 + \widetilde{s}_1 + \widetilde{s}_2. \tag{1.8b}$$

Recall the Gauss quadrature formula:

$$\int_{-1}^{1} f(t)\ \mathrm{d}\, t \approx \frac{8}{9} f(0) + \frac{5}{9}(f(\xi) + f(-\xi)), \quad \xi = \sqrt{\frac{3}{5}},$$

which is exact for quartic polynomials. An application of this formula simplifies the *mean value property* (1.3) into the form

$$\widetilde{\mu}(\widetilde{\mathbf{g}}_{2j-1}) + \widetilde{\mu}(\widetilde{\mathbf{g}}_{2j}) - 2\widetilde{\mu}(\widehat{\mathbf{m}}_j) = 0, \quad j = 1, \cdots, 4, \tag{1.9}$$

where

$$\begin{aligned}
&\widetilde{\mathbf{g}}_1 = \widehat{\mathbf{m}}_1 - \xi(\widehat{\mathbf{u}}_2 + \widetilde{\mathbf{s}}), \quad \widetilde{\mathbf{g}}_2 = \widehat{\mathbf{m}}_1 + \xi(\widehat{\mathbf{u}}_2 + \widetilde{\mathbf{s}}),\\
&\widetilde{\mathbf{g}}_3 = \widehat{\mathbf{m}}_2 + \xi(\widehat{\mathbf{u}}_1 + \widetilde{\mathbf{s}}), \quad \widetilde{\mathbf{g}}_4 = \widehat{\mathbf{m}}_2 - \xi(\widehat{\mathbf{u}}_1 + \widetilde{\mathbf{s}}),\\
&\widetilde{\mathbf{g}}_5 = \widehat{\mathbf{m}}_3 + \xi(\widehat{\mathbf{u}}_2 - \widetilde{\mathbf{s}}), \quad \widetilde{\mathbf{g}}_6 = \widehat{\mathbf{m}}_3 - \xi(\widehat{\mathbf{u}}_2 - \widetilde{\mathbf{s}}),\\
&\widetilde{\mathbf{g}}_7 = \widehat{\mathbf{m}}_4 - \xi(\widehat{\mathbf{u}}_1 - \widetilde{\mathbf{s}}), \quad \widetilde{\mathbf{g}}_8 = \widehat{\mathbf{m}}_4 + \xi(\widehat{\mathbf{u}}_1 - \widetilde{\mathbf{s}}),
\end{aligned}$$

together with $\widehat{\mathbf{m}}_j, j = 1, \cdots, 4$, are the twelve Gauss points on the edges. Here, and in what follows, we adopt the notations for the standard unit vectors: $\widehat{\mathbf{u}}_1 = \begin{pmatrix} 1 \\ 0 \end{pmatrix}$ and $\widehat{\mathbf{u}}_2 = \begin{pmatrix} 0 \\ 1 \end{pmatrix}$. Notice that the equations of lines for edges $\widetilde{\mathbf{e}}_j, j = 1, \cdots, 4$, are given in vector notation as follows:

$$\begin{aligned}
&\widetilde{\mathbf{e}}_1(t) = \widehat{\mathbf{m}}_1 + t(\widehat{\mathbf{u}}_2 + \widetilde{\mathbf{s}}), \quad \widetilde{\mathbf{e}}_2(t) = \widehat{\mathbf{m}}_2 + t(\widehat{\mathbf{u}}_1 + \widetilde{\mathbf{s}}),\\
&\widetilde{\mathbf{e}}_3(t) = \widehat{\mathbf{m}}_3 + t(\widehat{\mathbf{u}}_2 - \widetilde{\mathbf{s}}), \quad \widetilde{\mathbf{e}}_4(t) = \widehat{\mathbf{m}}_4 + t(\widehat{\mathbf{u}}_1 - \widetilde{\mathbf{s}}),
\end{aligned}$$

for $t \in [-1,1]$. Consider the quartic polynomial (1.7) restricted to an edge $\widetilde{\mathbf{e}}_j(t), t \in [-1,1]$. Since $\widetilde{\ell}_1\widetilde{\ell}_2$ is the product of two linear polynomials which vanishes at the other two end points of each edge, one sees that

$$\widetilde{\ell}_1(\widetilde{\mathbf{g}}_{2j-1})\widetilde{\ell}_2(\widetilde{\mathbf{g}}_{2j-1}) = \widetilde{\ell}_1(\widetilde{\mathbf{g}}_{2j})\widetilde{\ell}_2(\widetilde{\mathbf{g}}_{2j}) = (1-\xi^2)\widetilde{\ell}_1(\widehat{\mathbf{m}}_j)\widetilde{\ell}_2(\widehat{\mathbf{m}}_j), \quad \left(\xi = \sqrt{\frac{3}{5}}\right). \tag{1.10}$$

A combination of (1.9) and (1.10) yields that (1.3) holds if and only if the quadratic polynomial $\widetilde{\mathcal{Q}}$ satisfies

$$\widetilde{\mathcal{Q}}(\widetilde{\mathbf{g}}_{2j-1}) + \widetilde{\mathcal{Q}}(\widetilde{\mathbf{g}}_{2j}) - 5\widetilde{\mathcal{Q}}(\widehat{\mathbf{m}}_j) = 0, \quad j = 1, \cdots, 4. \tag{1.11}$$

A standard use of symbolic calculation gives the general solution of (1.11) in the following form

$$\widetilde{\mathcal{Q}}(\widetilde{\mathbf{x}}) = \left(\widetilde{x}_1 + \frac{2}{5}\widetilde{s}_2\right)^2 + \left(\widetilde{x}_2 + \frac{2}{5}\widetilde{s}_1\right)^2 - \widetilde{r}^2 + \widetilde{c}\left[(\widetilde{x}_1 + \frac{2}{5}\widetilde{s}_2)(\widetilde{x}_2 + \frac{2}{5}\widetilde{s}_1) + \frac{6}{25}\widetilde{s}_1\widetilde{s}_2\right], \tag{1.12}$$

with $\widetilde{r} = \frac{\sqrt{6}}{5}\sqrt{\frac{5}{2} - \widetilde{s}_1^2 - \widetilde{s}_2^2}$ for arbitrary constant $\widetilde{c} \in \mathbb{R}$. Here, we assume that the coefficient of $\widetilde{x}_1$ is normalized. Notice that $\widetilde{r}$ takes a positive real value if $\widetilde{K}$ is convex due to Remark 1.2.1.

Define, for each $\widetilde{c} \in \mathbb{R}$,

$$\widetilde{\mu}(\widetilde{x}_1, \widetilde{x}_2; \widetilde{c}) = -\frac{5}{3}\widetilde{\ell}_1(\widetilde{x}_1, \widetilde{x}_2)\widetilde{\ell}_2(\widetilde{x}_1, \widetilde{x}_2)\widetilde{\mathcal{Q}}(\widetilde{x}_1, \widetilde{x}_2),$$

where $\widetilde{\ell}_1$ and $\widetilde{\ell}_2$ are defined by (1.8) and $\widetilde{\mathcal{Q}}$ by (1.12) depending on $\widetilde{c}$ as well as $\widetilde{\mathbf{s}}$.

We are now in a position to define a class of *nonparametric nonconforming elements on the intermediate quadrilaterals* $\widetilde{K}$ with four degrees of freedom as follows.

1. $\widetilde{K} = \mathcal{S}_K(\widehat{K})$;

2. $\widetilde{P}_{\widetilde{K}}(\widetilde{c}) = \mathrm{Span}\{1, \widetilde{x}_1, \widetilde{x}_2, \widetilde{\mu}(\widetilde{x}_1, \widetilde{x}_2; \widetilde{c})\}$;

3. $\widetilde{\Sigma}_{\widetilde{K}} = \{\text{four edge-midpoint values of } \widetilde{K}\} = \{\text{four mean values over edges of } \widetilde{K}\}$.

By the above construction it is apparent that for any element $\widetilde{p} \in \widetilde{P}_{\widetilde{K}}(\widetilde{c})$ the *mean value property* holds:

$$\frac{1}{|\widetilde{e}_j|} \int_{\widetilde{e}_j} \widetilde{p}\, d\widetilde{\sigma} = \widetilde{p}(\widetilde{\mathbf{m}}_j), \qquad j = 1, 2, 3, 4.$$

Moreover, the above class of intermediate nonparametric elements is unisolvent for most of $\widetilde{c}$.

Theorem 1.2.2. *Assume that $\widetilde{c}$ is chosen such that $\widetilde{s}_1^2 + \widetilde{s}_2^2 + \frac{1}{3} + \widetilde{c}\,\widetilde{s}_1\widetilde{s}_2 \neq 0$. Then the intermediate nonparametric element $\left(\widetilde{K}, \widetilde{P}_{\widetilde{K}}(\widetilde{c}), \widetilde{\Sigma}_{\widetilde{K}}\right)$ is unisolvent.*

Proof. In order to show unisolvency of the space $\mathrm{Span}\{1, \widetilde{x}_1, \widetilde{x}_2, \widetilde{\mu}(\widetilde{x}_1, \widetilde{x}_2; \widetilde{c})\}$ with respect to the degrees of freedom $f(\widehat{\mathbf{m}}_j), j = 1, \cdots, 4$, denote the functions 1, $\widetilde{x}_1$, $\widetilde{x}_2$, and $\widetilde{\mu}(\widetilde{x}_1, \widetilde{x}_2; \widetilde{c})$ by $\widetilde{\phi_1}$, $\widetilde{\phi_2}$, $\widetilde{\phi_3}$, and $\widetilde{\phi_4}$, respectively and also define $A = (a_{jk}) \in M_{4\times 4}(\mathbb{R})$ by $a_{jk} = \widetilde{\phi_j}(\widehat{\mathbf{m}}_k)$. A symbolic calculation shows that $\det(A) = 16(\widetilde{s}_1^2 + \widetilde{s}_2^2 + \frac{1}{3} + \widetilde{c}\,\widetilde{s}_1\widetilde{s}_2)$, from which A is nonsingular for any $\widetilde{\mathbf{s}} \in \mathbb{R}^2$ if and only if $\widetilde{c}$ is chosen such that $\widetilde{s}_1^2 + \widetilde{s}_2^2 + \frac{1}{3} + \widetilde{c}\,\widetilde{s}_1\widetilde{s}_2 \neq 0$. This completes the proof. □

For $\widetilde{c} = 0$, the quadratic equation $\widetilde{\mathcal{Q}}(\widetilde{\mathbf{x}}) = 0$ denotes the circle with center $-\frac{2}{5}\begin{pmatrix}\widetilde{s}_2\\ \widetilde{s}_1\end{pmatrix}$ and radius $\widetilde{r}$. In this case, (1.12) can be easily derived by a geometric argument as follows. Indeed, assume that $\widetilde{\mathcal{Q}}(\widetilde{\mathbf{x}}) = 0$ denotes the circle with center $\mathbf{c} = \begin{pmatrix}c_1\\ c_2\end{pmatrix}$ and radius r so that $\widetilde{\mathcal{Q}}(\widetilde{\mathbf{x}}) = (\widetilde{\mathbf{x}} - \mathbf{c}) \cdot (\widetilde{\mathbf{x}} - \mathbf{c}) - r^2$. Then

(1.11) implies that

$$(\widetilde{\mathbf{g}}_{2j-1}-\mathbf{c})\cdot(\widetilde{\mathbf{g}}_{2j-1}-\mathbf{c})+(\widetilde{\mathbf{g}}_{2j}-\mathbf{c})\cdot(\widetilde{\mathbf{g}}_{2j}-\mathbf{c})-5(\widehat{\mathbf{m}}_j-\mathbf{c})\cdot(\widehat{\mathbf{m}}_j-\mathbf{c})=-3r^2,$$
$$j=1,\cdots,4.$$

Arrange these equations as follows:

$$(\mathbf{c}-\widetilde{\boldsymbol{\eta}}_{2j-1})\cdot(\mathbf{c}-\widetilde{\boldsymbol{\eta}}_{2j})=r^2,\quad j=1,\cdots,4, \tag{1.13}$$

where the points $\widetilde{\boldsymbol{\eta}}_{2j-1}$ and $\widetilde{\boldsymbol{\eta}}_{2j}$ are given between $\widetilde{\mathbf{g}}_{2j-1}$ and $\widehat{\mathbf{m}}_j$, and $\widetilde{\mathbf{g}}_{2j}$ and $\widehat{\mathbf{m}}_j$, respectively, explicitly defined as follows: with $\eta=\sqrt{\frac{2}{5}}$,

$$\begin{aligned}
&\widetilde{\boldsymbol{\eta}}_1=\widehat{\mathbf{m}}_1-\eta(\widehat{\mathbf{u}}_2+\widetilde{\mathbf{s}}),\quad \widetilde{\boldsymbol{\eta}}_2=\widehat{\mathbf{m}}_1+\eta(\widehat{\mathbf{u}}_2+\widetilde{\mathbf{s}}),\\
&\widetilde{\boldsymbol{\eta}}_3=\widehat{\mathbf{m}}_2+\eta(\widehat{\mathbf{u}}_1+\widetilde{\mathbf{s}}),\quad \widetilde{\boldsymbol{\eta}}_4=\widehat{\mathbf{m}}_2-\eta(\widehat{\mathbf{u}}_1+\widetilde{\mathbf{s}}),\\
&\widetilde{\boldsymbol{\eta}}_5=\widehat{\mathbf{m}}_3+\eta(\widehat{\mathbf{u}}_2-\widetilde{\mathbf{s}}),\quad \widetilde{\boldsymbol{\eta}}_6=\widehat{\mathbf{m}}_3-\eta(\widehat{\mathbf{u}}_2-\widetilde{\mathbf{s}}),\\
&\widetilde{\boldsymbol{\eta}}_7=\widehat{\mathbf{m}}_4-\eta(\widehat{\mathbf{u}}_1-\widetilde{\mathbf{s}}),\quad \widetilde{\boldsymbol{\eta}}_8=\widehat{\mathbf{m}}_4+\eta(\widehat{\mathbf{u}}_1-\widetilde{\mathbf{s}}).
\end{aligned}$$

Geometrically, (1.13) is equivalent to saying that the location of $\mathbf{c}$ is such that the four inner products of the vectors $\mathbf{c}-\widetilde{\boldsymbol{\eta}}_{2j-1}$ and $\mathbf{c}-\widetilde{\boldsymbol{\eta}}_{2j}$, for $j=1,\cdots,4$, are equal. It is straightforward from the equations (1.13) for $j=1$ and $j=3$ to see that $c_1=-\eta^2\widetilde{s}_2$, and similarly from those for $j=2$ and $j=4$ to see that $c_2=-\eta^2\widetilde{s}_1$. Then $r=\widetilde{r}$ follows immediately. Thus $\mathbf{c}$ and r are identical to the center and radius of the circle represented in (1.12) in the case of $\widetilde{c}=0$.

The global nonparametric quadrilateral nonconforming elements

Turn to the physical domain K. It is straightforward to define the finite elements from $\widetilde{K}$ to K by using the affine map $\mathcal{A}_K$ which enables the trans-

formed elements to retain the *mean value property* and unisolvency. A class of *nonparametric nonconforming elements on quadrilaterals* K with four degrees of freedom as follows.

1. $K = \mathcal{F}_K(\widehat{K})$;

2. $\mathcal{NC}_K = P_K(\widetilde{c}) = \mathrm{Span}\{1, x_1, x_2, \mu(x_1, x_2; \widetilde{c})\}$;

3. $\Sigma_K = \{\text{four edge-midpoint values of } K\} = \{\text{four mean values over edges of } K\}$,

where $\mu(x_1, x_2; \widetilde{c})$ is a quartic polynomial defined by $\mu(x_1, x_2; \widetilde{c}) = \widetilde{\mu} \circ \mathcal{A}_K^{-1}(x_1, x_2; \widetilde{c}) = -\frac{5}{3}\ell_1(x_1, x_2)\ell_2(x_1, x_2)q(x_1, x_2; \widetilde{c})$, with

$$\ell_1(\mathbf{x}) = \widetilde{\ell}_1 \circ \mathcal{A}_K^{-1}(\mathbf{x}), \quad \ell_2(\mathbf{x}) = \widetilde{\ell}_2 \circ \mathcal{A}_K^{-1}(\mathbf{x}), \quad q(\mathbf{x}; \widetilde{c}) = \widetilde{\Omega} \circ \mathcal{A}_K^{-1}(\mathbf{x}).$$

Notice that $\mu(\mathbf{x}; \widetilde{c})$ can be interpreted as a product of two linear polynomials and one quadratic polynomial such that the straight lines $\ell_1(\mathbf{x}) = 0$ and $\ell_2(\mathbf{x}) = 0$ are passing through $\mathbf{v}_1$, $\mathbf{v}_3$ and $\mathbf{v}_2$, $\mathbf{v}_4$, respectively and $q(\mathbf{x}; \widetilde{c}) = 0$ is an ellipse which is determined to satisfy the *mean value properties* for $\widetilde{\mu}(\widetilde{\mathbf{x}})$.

We now define the global nonparametric DSSY element spaces as follows

$$\mathcal{NC}_h^{np} = \{v_h \in L^2(\Omega) \mid v_h|_K \in \mathcal{NC}_K \text{ for } K \in \mathcal{T}_h, v_h \text{ is continuous at the midpoint of each } e \in \mathcal{E}_h\},$$

$$\mathcal{NC}_{h,0}^{np} = \{v_h \in \mathcal{NC}_h^{np} \mid v_h \text{ is zero at the midpoint of each } e \in \mathcal{E}_h \cap \partial\Omega\}.$$

Remark 1.2.3. *Since these new finite element spaces have the mean value property as in [8], clearly the optimal convergence order is guaranteed for solving second-order elliptic problems. Indeed,* (1.3) *implies the pass of a patch test against constant functions on each interior edge (see (2.7a) and (2.7b) of [8]), which in turn implies the following bound of the consistent error term in the*

second Strang lemma:

$$\sup_{w_h \in \mathcal{NC}_{h,0}^{np}} \frac{|a_h(u, w_h) - (f, w_h)|}{\|w_h\|_{1,h}} \leq C\|u\|_2 h,$$

where $u \in H^2(\Omega) \cap H_0^1(\Omega)$ *is a solution to* $a(u, v) = (f, v)\ \forall v \in H_0^1(\Omega)$, *and* $a(\cdot, \cdot)$ *and* $a_h(\cdot, \cdot)$ *are bounded, coercive bilinear forms on* $H_0^1(\Omega)$ *and* $\mathcal{NC}_{h,0}^{np}$, *respectively.*

Remark 1.2.4. *The new nonparametric DSSY elements will be used as a stable family of mixed finite elements for the velocity fields, combined with the piecewise constant element for pressure, in solving the Navier-Stokes equations [5, 12, 22]. The nonconforming nature enables us to solve elasticity problems without numerical locking, either [16, 27]. See the numerical experiments in Subsections 3.2 and 3.3.*

Remark 1.2.5. *In practice, the choice* $\widetilde{c} = 0$ *is recommended since it minimizes the number of computations in applying quadrature rules.*

Remark 1.2.6. *One may construct basis functions in a sixth-degree polynomial space other than the quartic polynomial as in* (1.2) *following the same idea. However, using a higher-degree polynomial space requires a higher accuracy quadrature rule in the construction of the stiffness matrix. In this sense, the quartic polynomial space seems to be a reasonable choice in view of implementation issues.*

1.3 Numerical results

1.3.1 The elliptic problem

In this section we perform numerical experiments for a simple elliptic problem:

$$\begin{aligned} -\Delta u &= f \qquad \text{in } \Omega, \\ u &= 0 \qquad \text{on } \partial\Omega, \end{aligned}$$

on the domain $\Omega = (0,1)^2$. The source function f is given so that the exact solution is

$$u(\mathbf{x}) = \sin \pi x_1 \sin \pi x_2.$$

We consider two kinds of elements: the parametric DSSY element $\mathcal{NC}^p_{h,0}$, and the nonparametric DSSY elements $\mathcal{NC}^{np}_{h,0}$ with $\widetilde{c} = 0$ and $\widetilde{c} = 1$. Also two types of quadrilateral meshes were employed: uniformly θ-dependent quadrilateral meshes as shown in Figure 3.1 are used and the randomly perturbed quadrilateral meshes depicted in Figure 1.3. The uniformly θ-dependent quadrilaterals become rectangles if $\theta = 0$, while they degenerate into triangles if $\theta = 1$.

The tables containing numerical results are organized as follows: the parametric nonconforming elements in Tables 1.7 and 1.10, the nonparametric nonconforming elements with $\widetilde{c} = 0$ in Tables 1.8 and 1.11, and those with $\widetilde{c} = 1$ in Tables 1.9 and 1.12; the uniformly θ-dependent trapezoidal meshes in Tables 1.7 – 1.9 and the nonuniform quadrilateral meshes in Tables 1.10 – 1.12.

We tested several different θ's, but the convergence behaviors were quite similar and thus we report only the case of $\theta = 0.7$.

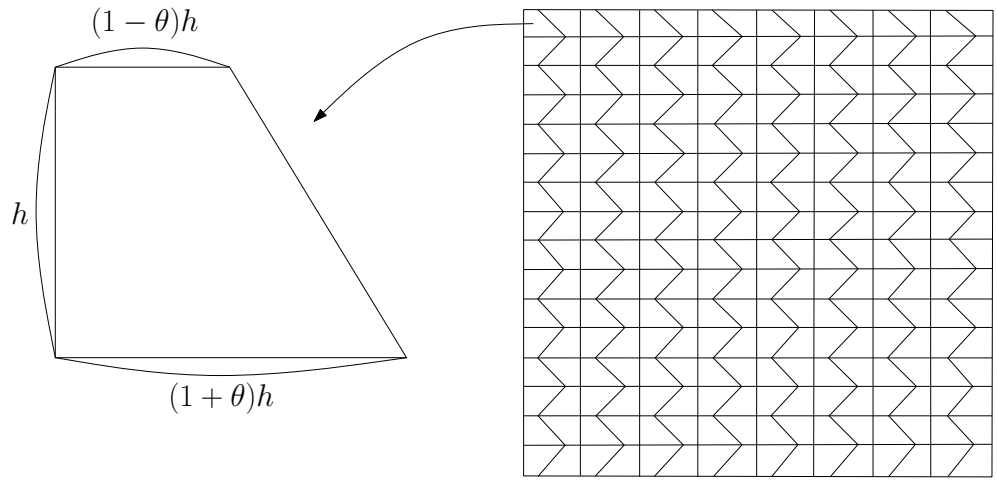

Figure 1.2: A uniform trapezoidal triangulation with a trapezoidal with parameter $0 \leq \theta < 1$.

Numerical experiments were performed with increasing values of $\widetilde{c}$ such as 10, 100, 1000, and so on. The larger $\widetilde{c}$ values are chosen, the slower convergence was observed. We only present numerics for the two nonparametric elements with $\widetilde{c} = 0$ and 1. At this point we recommend readers to use $\widetilde{c} = 0$ for its simplicity.

As observed in the uniform mesh the convergence order is optimal for both elements and the values of numerical solutions are almost identical. In order to compare cost efficiency in a fair fashion, we computed nonparametric basis functions for each quadrilateral and applied the static condensation to circumvent bubble functions for parametric element also for each quadrilateral. From Table 1.13 we observe that when the mesh size h is larger than $1/100$, the nonparametric element is cheaper to use; however, the computing time ratios approach to 1 (still the use of nonparametric element seems to be cheaper), as the mesh size tends to decrease. These phenomena are perhaps due to the fact that the additional cost in static condensation for the parametric elements takes a less portion in the total computing time as the mesh size decreases.

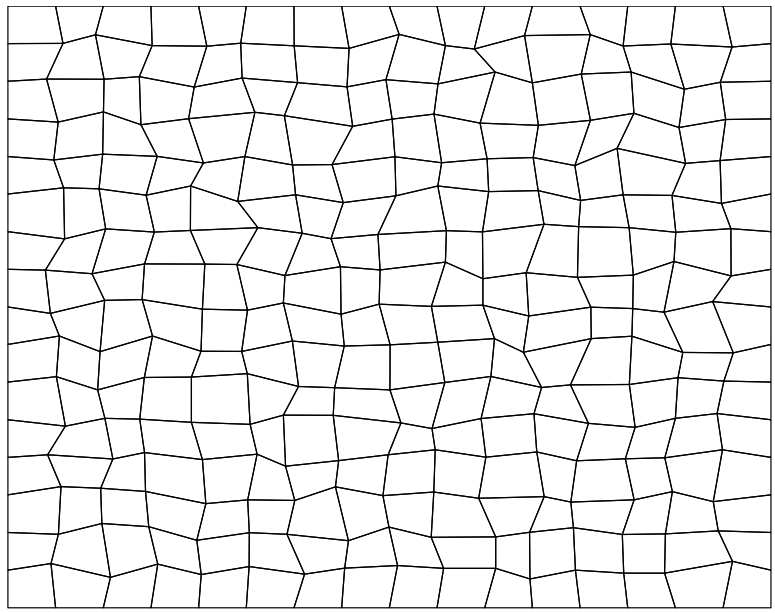

Figure 1.3: A nonuniform randomly perturbed quadrilateral triangulation

1.3.2 The incompressible Stokes equations

In this subsection, we apply $\mathcal{NC}_{h,0}^{np}$ to approximate each component of the velocity fields in solving the incompressible Stokes equations in two dimensions, while the piecewise constant element is employed to approximate the pressure.

Set $\Omega = (0,1)^2$ and consider the following Stokes equations:

$$\begin{aligned} -\Delta \mathbf{u} + \nabla p &= \mathbf{f} \qquad \text{in } \Omega, \\ \nabla \cdot \mathbf{u} &= 0 \qquad \text{in } \Omega, \\ \mathbf{u} &= 0 \qquad \text{on } \partial\Omega, \end{aligned}$$

h	DOF	$\|\|u-u_h\|\|_{0,\Omega}$	ratio	$\|\|u-u_h\|\|_{1,h}$	ratio
1/4	40	0.3365E-01	-	0.7198	-
1/8	176	0.9423E-02	1.84	0.3732	0.95
1/16	736	0.2511E-02	1.90	0.1895	0.98
1/32	3008	0.6483E-03	1.95	0.9533E-01	0.99
1/64	12160	0.1646E-03	1.98	0.4779E-01	1.00
1/128	48896	0.4146E-04	1.99	0.2393E-01	1.00
1/256	196096	0.1040E-04	1.99	0.1197E-01	1.00

Table 1.1: Computational results for $\mathcal{NC}^p_{h,0}$ with $\theta = 0.3$ for the elliptic problem.

h	DOF	$\|\|u-u_h\|\|_{0,\Omega}$	ratio	$\|\|u-u_h\|\|_{1,h}$	ratio
1/4	24	0.3433E-01	-	0.7306	-
1/8	112	0.9427E-02	1.86	0.3733	0.97
1/16	480	0.2504E-02	1.91	0.1889	0.98
1/32	1984	0.6479E-03	1.95	0.9506E-01	0.99
1/64	8064	0.1648E-03	1.98	0.4767E-01	1.00
1/128	32512	0.4155E-04	1.99	0.2387E-01	1.00
1/256	130560	0.1043E-04	1.99	0.1194E-01	1.00

Table 1.2: Computational results for $\mathcal{NC}^{np}_{h,0}$ with $\theta = 0.3$ and $\widetilde{c} = 0$ for the elliptic problem.

where the force term $\mathbf{f}$ is generated by the following exact solution

$$\mathbf{u}(x_1,x_2) = \begin{pmatrix} e^{x_1+2x_2}(x_1^4-2x_1^3+x_1^2)(2x_2^4-4x_2^2+2x_2) \\ -e^{x_1+2x_2}(x_1^4+2x_1^3-5x_1^2+2x_1)(x_2^4-2x_2^3+x_2^2) \end{pmatrix},$$

$$p(x_1,x_2) = -\sin 2\pi x_1 \sin 2\pi x_2.$$

Table 1.14 shows the numerical results on uniform trapezoidal meshes with $\theta = 0.7$ and $\widetilde{c} = 0$. Similarly, Table 1.16 presents the results on the perturbed nonuniform meshes with $\widetilde{c} = 0$. From these numerical results, we observe the optimal convergence rates of $O(h^2)$ and $O(h)$ for the velocity and pressure in

h	DOF	$\|\|u-u_h\|\|_{0,\Omega}$	ratio	$\|\|u-u_h\|\|_{1,h}$	ratio
1/4	24	0.3690E-01	-	0.7402	-
1/8	112	0.9998E-02	1.88	0.3832	0.95
1/16	480	0.2617E-02	1.93	0.1929	0.99
1/32	1984	0.6892E-03	1.92	0.9747E-01	0.98
1/64	8064	0.1767E-03	1.96	0.4903E-01	1.00
1/128	32512	0.4486E-04	1.98	0.2457E-01	1.00
1/256	130560	0.1129E-04	1.99	0.1231E-01	1.00

Table 1.3: Computational results for $\mathcal{NC}_{h,0}^{np}$ with $\theta = 0.3$ and $\widetilde{c} = 1$ for the elliptic problem.

h	DOF	$\|\|u-u_h\|\|_{0,\Omega}$	ratio	$\|\|u-u_h\|\|_{1,h}$	ratio
1/4	40	0.4091E-01	-	0.7742	-
1/8	176	0.1206E-01	1.76	0.4045	0.94
1/16	736	0.3291E-02	1.87	0.2066	0.97
1/32	3008	0.8618E-03	1.93	0.1043	0.99
1/64	12160	0.2205E-03	1.97	0.5239E-01	0.99
1/128	48896	0.5573E-04	1.98	0.2625E-01	1.00
1/256	196096	0.1401E-04	1.99	0.1314E-01	1.00

Table 1.4: Computational results for $\mathcal{NC}_{h,0}^{p}$ with $\theta = 0.5$ for the elliptic problem.

L^2 norm, respectively. The numerical solutions in the case with $\widetilde{c} \neq 0$ behave similarly, whose tables are omitted to report.

1.3.3 The planar linear elasticity problem

In this subsection, the nonparametric element $\mathcal{NC}_{h,0}^{np}$ is applied to approximate each component of the displacement fields for the planar linear elasticity problem with the clamped boundary condition.

Set $\Omega = (0,1)^2$. For $(\mu, \lambda) \in [\mu_0, \mu_1] \times [\lambda_1, \infty)$, consider the following

h	DOF	$\|\|u-u_h\|\|_{0,\Omega}$	ratio	$\|\|u-u_h\|\|_{1,h}$	ratio
1/4	24	0.4175E-01	-	0.7690	-
1/8	112	0.1205E-01	1.79	0.3984	0.95
1/16	480	0.3263E-02	1.88	0.2039	0.97
1/32	1984	0.8577E-03	1.93	0.1032	0.98
1/64	8064	0.2202E-03	1.96	0.5192E-01	0.99
1/128	32512	0.5580E-04	1.98	0.2604E-01	1.00
1/256	130560	0.1404E-04	1.99	0.1304E-01	1.00

Table 1.5: Computational results for $\mathcal{NC}_{h,0}^{np}$ with $\theta = 0.5$ and $\widetilde{c} = 0$ for the elliptic problem.

h	DOF	$\|\|u-u_h\|\|_{0,\Omega}$	ratio	$\|\|u-u_h\|\|_{1,h}$	ratio
1/4	24	0.4415E-01	-	0.7816	-
1/8	112	0.1256E-01	1.81	0.4093	0.93
1/16	480	0.3318E-02	1.92	0.2072	0.98
1/32	1984	0.8795E-03	1.92	0.1051	0.98
1/64	8064	0.2268E-03	1.96	0.5294E-01	0.99
1/128	32512	0.5769E-04	1.98	0.2655E-01	1.00
1/256	130560	0.1455E-04	1.99	0.1330E-01	1.00

Table 1.6: Computational results for $\mathcal{NC}_{h,0}^{np}$ with $\theta = 0.5$ and $\widetilde{c} = 1$ for the elliptic problem.

elasticity equations with homogeneous boundary condition:

$$\begin{aligned} -(\lambda+\mu)\nabla(\nabla\cdot\mathbf{u}) - \mu\Delta\mathbf{u} &= \mathbf{f} \qquad \text{in } \Omega, \\ \mathbf{u} &= 0 \qquad \text{on } \partial\Omega, \end{aligned}$$

where the external force term $\mathbf{f}$ is generated by the following exact solution

$$\begin{aligned} u_1(x_1,x_2) &= \sin 2\pi x_2(-1+\cos 2\pi x_1) + \frac{1}{1+\lambda}\sin\pi x_1 \sin\pi x_2, \\ u_2(x_1,x_2) &= -\sin 2\pi x_1(-1+\cos 2\pi x_2) + \frac{1}{1+\lambda}\sin\pi x_1 \sin\pi x_2. \end{aligned}$$

In order to check numerical locking phenomena, the Lamé parameters are

h	DOF	$\|\|u-u_h\|\|_{0,\Omega}$	ratio	$\|\|u-u_h\|\|_{1,h}$	ratio
1/4	40	0.5284E-01	-	0.8532	-
1/8	176	0.1556E-01	1.76	0.4458	0.94
1/16	736	0.4184E-02	1.89	0.2274	0.97
1/32	3008	0.1096E-02	1.93	0.1147	0.99
1/64	12160	0.2810E-03	1.96	0.5756E-01	0.99
1/128	48896	0.7117E-04	1.98	0.2883E-01	1.00
1/256	196096	0.1791E-04	1.99	0.1443E-01	1.00

Table 1.7: Computational results for $\mathcal{NC}^p_{h,0}$ with $\theta = 0.7$ for the elliptic problem.

h	DOF	$\|\|u-u_h\|\|_{0,\Omega}$	ratio	$\|\|u-u_h\|\|_{1,h}$	ratio
1/4	24	0.5437E-01	-	0.8221	-
1/8	112	0.1568E-01	1.79	0.4302	0.93
1/16	480	0.4145E-02	1.92	0.2213	0.96
1/32	1984	0.1084E-02	1.93	0.1124	0.98
1/64	8064	0.2788E-03	1.96	0.5659E-01	0.99
1/128	32512	0.7077E-04	1.98	0.2839E-01	1.00
1/256	130560	0.1783E-04	1.99	0.1422E-01	1.00

Table 1.8: Computational results for $\mathcal{NC}^{np}_{h,0}$ with $\theta = 0.7$ and $\widetilde{c} = 0$ for the elliptic problem

chosen such that $(\mu, \lambda) = (1, 1)$ and $(1, 10^5)$. The numerical results are presented in Tables 1.18 and 1.19 for both cases on uniform trapezoidal meshes with $\theta = 0.7$ and $\widetilde{c} = 0$. Similar results are given in Tables 1.20 and 1.21 for both cases on the randomly perturbed meshes with $\widetilde{c} = 0$. One can easily observe from the numerical results that the nonparametric element $\mathcal{NC}^{np}_{h,0}$ can be used to solve planar elasticity problems with the clamped boundary condition optimally without numerical locking.

h	DOF	$\|\|u-u_h\|\|_{0,\Omega}$	ratio	$\|\|u-u_h\|\|_{1,h}$	ratio
1/4	24	0.5840E-01	-	0.8486	-
1/8	112	0.1655E-01	1.82	0.4452	0.93
1/16	480	0.4229E-02	1.97	0.2261	0.98
1/32	1984	0.1102E-02	1.94	0.1145	0.98
1/64	8064	0.2836E-03	1.96	0.5760E-01	0.99
1/128	32512	0.7212E-04	1.98	0.2887E-01	1.00
1/256	130560	0.1819E-04	1.99	0.1446E-01	1.00

Table 1.9: Computational results for $\mathcal{NC}_{h,0}^{np}$ with $\theta = 0.7$ and $\widetilde{c} = 1$ for the elliptic problem.

h	DOF	$\|\|u-u_h\|\|_{0,\Omega}$	ratio	$\|\|u-u_h\|\|_{1,h}$	ratio
1/4	40	0.3490E-01	-	0.7183	-
1/8	176	0.8663E-02	2.01	0.3657	0.97
1/16	736	0.2287E-02	1.92	0.1871	0.97
1/32	3008	0.5835E-03	1.97	0.9387E-01	0.99
1/64	12160	0.1481E-03	1.98	0.4721E-01	0.99
1/128	48896	0.3729E-04	1.99	0.2363E-01	1.00
1/256	196096	0.9350E-05	2.00	0.1183E-01	1.00

Table 1.10: Computational results for $\mathcal{NC}_{h,0}^{p}$ on the nonuniform randomly perturbed meshes for the elliptic problem.

h	DOF	$\|\|u-u_h\|\|_{0,\Omega}$	ratio	$\|\|u-u_h\|\|_{1,h}$	ratio
1/4	24	0.3594E-01	-	0.7363	-
1/8	112	0.8760E-02	2.04	0.3682	1.00
1/16	480	0.2290E-02	1.94	0.1873	0.98
1/32	1984	0.5834E-03	1.97	0.9386E-01	1.00
1/64	8064	0.1479E-03	1.98	0.4718E-01	0.99
1/128	32512	0.3725E-04	1.99	0.2362E-01	1.00
1/256	130560	0.9341E-05	2.00	0.1182E-01	1.00

Table 1.11: Computational results for $\mathcal{NC}_{h,0}^{np}$ on the nonuniform randomly perturbed meshes when $\widetilde{c} = 0$ for the elliptic problem.

h	DOF	$\|\|u-u_h\|\|_{0,\Omega}$	ratio	$\|\|u-u_h\|\|_{1,h}$	ratio
1/4	24	0.3598E-01	-	0.7370	-
1/8	112	0.8752E-02	2.04	0.3684	1.00
1/16	480	0.2290E-02	1.93	0.1874	0.98
1/32	1984	0.5842E-03	1.97	0.9398E-01	1.00
1/64	8064	0.1481E-03	1.98	0.4725E-01	0.99
1/128	32512	0.3730E-04	1.99	0.2365E-01	1.00
1/256	130560	0.9353E-05	2.00	0.1184E-01	1.00

Table 1.12: Computational results for $\mathcal{NC}^{np}_{h,0}$ on the nonuniform randomly perturbed meshes when $\widetilde{c}=1$ for the elliptic problem.

h	$\theta=0.3$	$\theta=0.5$	$\theta=0.7$	Random mesh
1/8	0.6764	0.6764	0.6666	0.6571
1/16	0.6711	0.6621	0.6802	0.6712
1/32	0.6796	0.6761	0.6844	0.7022
1/64	0.7333	0.7285	0.7303	0.7344
1/128	0.7611	0.7656	0.7540	0.7275
1/256	0.8136	0.8296	0.7924	0.7875
1/512	0.9431	0.9170	0.8861	0.8415

Table 1.13: Ratio of computing time $\mathrm{t}(\mathcal{NC}^{np}_{h,0})/\mathrm{t}(\mathcal{NC}^{p}_{h,0})$ for the elliptic problem on uniform trapezoidal meshes with varying parameter θ and on nonuniform randomly perturbed meshes.

h	DOF	$\|\|\mathbf{u}-\mathbf{u}_h\|\|_{0,\Omega}$	ratio	$\|\|p-p_h\|\|_{0,\Omega}$	ratio
1/4	63	0.1302E-01	-	0.2770	-
1/8	287	0.5424E-02	1.26	0.1898	0.55
1/16	1215	0.1631E-02	1.73	0.9571E-01	0.99
1/32	4991	0.4396E-03	1.89	0.4801E-01	1.00
1/64	20223	0.1130E-03	1.96	0.2410E-01	0.99
1/128	81407	0.2855E-04	1.98	0.1208E-01	1.00

Table 1.14: Computational results for $\mathcal{NC}^{np}_{h,0}$ with $\theta=0.7$ and $\widetilde{c}=0$ for the Stokes problem.

h	DOF	$\|\|\mathbf{u}-\mathbf{u}_h\|\|_{0,\Omega}$	ratio	$\|\|p-p_h\|\|_{0,\Omega}$	ratio
1/4	63	0.1368E-01	-	0.2775	-
1/8	287	0.5379E-02	1.35	0.1913	0.54
1/16	1215	0.1618E-02	1.73	0.9604E-01	0.99
1/32	4991	0.4388E-03	1.88	0.4801E-01	1.00
1/64	20223	0.1131E-03	1.96	0.2409E-01	1.00
1/128	81407	0.2858E-04	1.98	0.1208E-01	1.00

Table 1.15: Computational results for $\mathcal{NC}_{h,0}^{np}$ with $\theta = 0.7$ and $\widetilde{c} = 1$ for the Stokes problem.

h	DOF	$\|\|\mathbf{u}-\mathbf{u}_h\|\|_{0,\Omega}$	ratio	$\|\|p-p_h\|\|_{0,\Omega}$	ratio
1/4	63	0.1205E-01	-	0.2960	-
1/8	287	0.3474E-02	1.79	0.1635	0.85
1/16	1215	0.9061E-03	1.94	0.8381E-01	0.96
1/32	4991	0.2332E-03	1.96	0.4216E-01	0.99
1/64	20223	0.5801E-04	2.00	0.2103E-01	1.00
1/128	81407	0.1455E-04	2.00	0.1052E-01	1.00

Table 1.16: Computational results for $\mathcal{NC}_{h,0}^{np}$ on the perturbed nonuniform mesh when $\widetilde{c} = 0$ for the Stokes problem.

h	DOF	$\|\|\mathbf{u}-\mathbf{u}_h\|\|_{0,\Omega}$	ratio	$\|\|p-p_h\|\|_{0,\Omega}$	ratio
1/4	63	0.1229E-01	-	0.2978	-
1/8	287	0.3606E-02	1.77	0.1642	0.86
1/16	1215	0.9423E-03	1.94	0.8391E-01	0.97
1/32	4991	0.2423E-03	1.96	0.4219E-01	0.99
1/64	20223	0.6015E-04	2.01	0.2104E-01	1.00
1/128	81407	0.1509E-04	2.00	0.1052E-01	1.00

Table 1.17: Computational results for $\mathcal{NC}_{h,0}^{np}$ on the perturbed nonuniform mesh when $\widetilde{c} = 1$ for the Stokes problem.

h	DOF	$\|\|\mathbf{u}-\mathbf{u}_h\|\|_{0,\Omega}$	ratio	$\|\|\mathbf{u}-\mathbf{u}_h\|\|_{1,h}$	ratio
1/4	48	0.3787	-	5.640	-
1/8	224	0.1074	1.81	2.941	0.93
1/16	960	0.2911E-01	1.88	1.524	0.94
1/32	3968	0.7521E-02	1.95	0.7712	0.98
1/64	16128	0.1906E-02	1.98	0.3870	0.99
1/128	65024	0.4793E-03	1.99	0.1937	1.00

Table 1.18: Computational results for $\mathcal{NC}_{h,0}^{np}$ with $\theta = 0.7$, $\widetilde{c} = 0$, $\mu = 1$, and $\lambda = 1$ for the elasticity problem.

h	DOF	$\|\|\mathbf{u}-\mathbf{u}_h\|\|_{0,\Omega}$	ratio	$\|\|\mathbf{u}-\mathbf{u}_h\|\|_{1,h}$	ratio
1/4	48	0.3781	-	5.631	-
1/8	224	0.1075	1.81	2.918	0.95
1/16	960	0.2900E-01	1.89	1.511	0.95
1/32	3968	0.7495E-02	1.95	0.7642	0.98
1/64	16128	0.1902E-02	1.98	0.3834	0.99
1/128	65024	0.4789E-03	1.99	0.1919	1.00

Table 1.19: Computational results for $\mathcal{NC}_{h,0}^{np}$ with $\theta = 0.7$, $\widetilde{c} = 0$, $\mu = 1$, and $\lambda = 10^5$ for the elasticity problem.

h	DOF	$\|\|\mathbf{u}-\mathbf{u}_h\|\|_{0,\Omega}$	ratio	$\|\|\mathbf{u}-\mathbf{u}_h\|\|_{1,h}$	ratio
1/4	48	0.2517	-	4.679	-
1/8	224	0.6530E-01	1.77	2.459	0.73
1/16	960	0.1724E-01	1.92	1.264	0.96
1/32	3968	0.4392E-02	1.97	0.6382	0.99
1/64	16128	0.1105E-02	1.99	0.3197	1.00
1/128	65024	0.2776E-03	1.99	0.1601	1.00

Table 1.20: Computational results for $\mathcal{NC}_{h,0}^{np}$ on the perturbed nonuniform mesh with $\widetilde{c} = 0$, $\mu = 1$, and $\lambda = 1$ for the elasticity problem.

h	DOF	$\|\|\mathbf{u}-\mathbf{u}_h\|\|_{0,\Omega}$	ratio	$\|\|\mathbf{u}-\mathbf{u}_h\|\|_{1,h}$	ratio
1/4	48	0.2523	-	4.659	-
1/8	224	0.6591E-01	1.93	2.444	0.93
1/16	960	0.1746E-01	1.92	1.255	0.96
1/32	3968	0.4461E-02	1.97	0.6334	0.99
1/64	16128	0.1124E-02	1.99	0.3174	1.00
1/128	65024	0.2825E-03	1.99	0.1589	1.00

Table 1.21: Computational results for $\mathcal{NC}_{h,0}^{np}$ on the perturbed nonuniform mesh with $\widetilde{c}=0$, $\mu=1$, and $\lambda=10^5$ for the elasticity problem.

Chapter 2

Three-dimensional nonparametric DSSY elements

2.1 Introduction

In three dimensional domain, the hexahedral meshes are widely used in the finite element method. The parametric DSSY element for the hexahedral mesh was introduced in [8]. However its convergence order of the numerical solution can be affected by the shape of hexahedral mesh, that is, in the parallelepiped mesh, the three dimensional parametric DSSY element has always the optimal convergence property of numerical solution, but may not in genuinely hexahedral meshes (one of the pairs of faced two faces of a hexehedron is not parallel). In this chapter a class of nonparametric nonconforming hexahedral finite elements with six degrees of freedom will be introduced which has optimal order of convergence for genuinely hexahedral meshes (consisting of six flat faces) and we deal with the case of non-flat hexahedron mesh by

defining a finite element space which has twelve local basis functions. As in Chapter 1, we use decomposition of a tilinear map into a simple tilinear map followed by an affine map. Also, we introduce a linearized map for the tilinear map and define a new finite element space such that the geometrical variety of mesh is guaranteed.

2.2 3D nonparametric DSSY elements

2.2.1 Intermediate Spaces

Set $\widehat{K} = [-1,1]^3$ and employ the following notations to denote the eight vertices:

$$\widehat{\mathbf{V}}_{jkl}, \quad j,k,l \in \{-1,1\}.$$

Then the trilinear basis functions $\phi_{jkl}(\widehat{\mathbf{x}}), j,k,l \in \{-1,1\}$, such that

$$\phi_{jkl}(\widehat{\mathbf{V}}_{j'k'l'}) = \delta_{jj'}\delta_{kk'}\delta_{ll'}, \quad j',k',l' \in \{-1,1\}$$

are given by

$$\phi_{jkl}(\widehat{\mathbf{x}}) = \frac{1}{8}(1+j\widehat{x}_1)(1+k\widehat{x}_2)(1+l\widehat{x}_3), \quad j,k,l \in \{-1,1\}.$$

Hence a trilinear map which maps $\widehat{\mathbf{V}}_{jkl}$, $j,k,l \in \{-1,1\}$, to $\mathbf{V}_{jkl}$, $j,k,l \in \{-1,1\}$, respectively, is given by

$$\mathcal{F}_K(\widehat{\mathbf{x}}) = \frac{1}{8} \sum_{j,k,l \in \{-1,1\}} (1+j\widehat{x}_1)(1+k\widehat{x}_2)(1+l\widehat{x}_3)\mathbf{V}_{jkl}.$$

Notice that the above trilinear map can be written as

$$\mathcal{F}_K(\widehat{\mathbf{x}}) = \mathbf{b} + \mathbf{A}_1\widehat{x}_1 + \mathbf{A}_2\widehat{x}_2 + \mathbf{A}_3\widehat{x}_3 + \mathbf{A}_4\widehat{x}_2\widehat{x}_3 + \mathbf{A}_5\widehat{x}_3\widehat{x}_1 + \mathbf{A}_6\widehat{x}_1\widehat{x}_2 + \mathbf{A}_7\widehat{x}_1\widehat{x}_2\widehat{x}_3,$$

where $\mathbf{b}, \mathbf{A}_j, j = 1, \cdots, 7$, are three dimensional vectors. Indeed, these vectors are given in terms of the deformed vectors $\mathbf{V}_{jkl} = \mathcal{F}_K(\widehat{\mathbf{V}}_{jkl}), j, k, l \in \{-1, 1\}$, by the following formula:

$$\begin{aligned}
\mathbf{b} &= \frac{1}{8}\sum_{j,k,l\in\{-1,1\}} \mathbf{V}_{jkl}; \qquad \mathbf{A}_1 = \frac{1}{8}\sum_{j,k,l\in\{-1,1\}} j\mathbf{V}_{jkl};\\
\mathbf{A}_2 &= \frac{1}{8}\sum_{j,k,l\in\{-1,1\}} k\mathbf{V}_{jkl}; \quad \mathbf{A}_3 = \frac{1}{8}\sum_{j,k,l\in\{-1,1\}} l\mathbf{V}_{jkl};\\
\mathbf{A}_4 &= \frac{1}{8}\sum_{j,k,l\in\{-1,1\}} kl\mathbf{V}_{jkl}; \quad \mathbf{A}_5 = \frac{1}{8}\sum_{j,k,l\in\{-1,1\}} lj\mathbf{V}_{jkl};\\
\mathbf{A}_6 &= \frac{1}{8}\sum_{j,k,l\in\{-1,1\}} jk\mathbf{V}_{jkl}; \quad \mathbf{A}_7 = \frac{1}{8}\sum_{j,k,l\in\{-1,1\}} jkl\mathbf{V}_{jkl}.
\end{aligned}$$

Assume that

$$\mathbb{A} = \begin{pmatrix} \mathbf{A}_1 & \mathbf{A}_2 & \mathbf{A}_3 \end{pmatrix}$$

is an invertible 3×3 matrix. Then $\mathcal{A}_K : \mathbb{R}^3 \to \mathbb{R}^3$ defined by

$$\mathcal{A}_K\widetilde{\mathbf{x}} = \mathbb{A}\widetilde{\mathbf{x}} + \mathbf{b}$$

is an affine map and $\mathcal{S}_K : \mathbb{R}^3 \to \mathbb{R}^3$ defined by

$$\mathcal{S}_K\widehat{\mathbf{x}} = \widehat{\mathbf{x}} + \widehat{x}_2\widehat{x}_3\mathbb{A}^{-1}\mathbf{A}_4 + \widehat{x}_3\widehat{x}_1\mathbb{A}^{-1}\mathbf{A}_5 + \widehat{x}_1\widehat{x}_2\mathbb{A}^{-1}\mathbf{A}_6 + \widehat{x}_1\widehat{x}_2\widehat{x}_3\mathbb{A}^{-1}\mathbf{A}_7,$$

is a *simple trilinear map* such that

$$\mathcal{F}_K = \mathcal{A}_K \circ \mathcal{S}_K.$$

By a simple trilinear map, we mean it is a perturbation of identity by a nonlinear mapping which consists of only trilinear parts. Denote

$$\widetilde{\mathbf{s}}_m = \mathbb{A}^{-1}\mathbf{A}_{3+m}, \quad m = 1, \cdots, 4.$$

Then these four vectors represent relative deformation as follows:

$$\mathcal{S}_K\widehat{\mathbf{x}} = \widehat{\mathbf{x}} + \widehat{x}_2\widehat{x}_3\widetilde{\mathbf{s}}_1 + \widehat{x}_3\widehat{x}_1\widetilde{\mathbf{s}}_2 + \widehat{x}_1\widehat{x}_2\widetilde{\mathbf{s}}_3 + \widehat{x}_1\widehat{x}_2\widehat{x}_3\widetilde{\mathbf{s}}_4. \tag{2.1}$$

The *simple trilinear map* $\mathcal{S}_K$ transforms $\widehat{\mathbf{V}}_{jkl}$ to $\widetilde{\mathbf{V}}_{jkl}$ for $j, k, l \in \{-1, 1\}$ as follows:

$$\widetilde{\mathbf{V}}_{jkl} = \widehat{\mathbf{V}}_{jkl} + \widetilde{\mathbf{d}}_{jkl} \qquad \text{for } j, k, l \in \{-1, 1\},$$

where the *deformation vector* $\widetilde{\mathbf{d}}_{jkl}$'s are given by

$$\widetilde{\mathbf{d}}_{jkl} = kl\widetilde{\mathbf{s}}_1 + lj\widetilde{\mathbf{s}}_2 + jk\widetilde{\mathbf{s}}_3 + jkl\widetilde{\mathbf{s}}_4 \qquad \text{for } j, k, l \in \{-1, 1\}. \tag{2.2}$$

Let us take a look at the image of the surface $\{\widehat{x}_3 = 1\}$. In this case, $l = 1$ is fixed in (2.2) and $\widetilde{\mathbf{d}}_{jk1}, j, k \in \{-1, 1\}$, are given as follows:

$$\begin{aligned} \widetilde{\mathbf{d}}_{1,1,l} &= \widetilde{\mathbf{s}}_1 + \widetilde{\mathbf{s}}_2 + \widetilde{\mathbf{s}}_3 + \widetilde{\mathbf{s}}_4; \qquad \widetilde{\mathbf{d}}_{-1,1,l} = \widetilde{\mathbf{s}}_1 - \widetilde{\mathbf{s}}_2 - \widetilde{\mathbf{s}}_3 - \widetilde{\mathbf{s}}_4; \\ \widetilde{\mathbf{d}}_{-1,-1,l} &= -\widetilde{\mathbf{s}}_1 - \widetilde{\mathbf{s}}_2 + \widetilde{\mathbf{s}}_3 + \widetilde{\mathbf{s}}_4; \qquad \widetilde{\mathbf{d}}_{1,-1,l} = -\widetilde{\mathbf{s}}_1 + \widetilde{\mathbf{s}}_2 - \widetilde{\mathbf{s}}_3 - \widetilde{\mathbf{s}}_4. \end{aligned} \tag{2.3}$$

Notice that the deformation vector from $\widehat{\mathbf{v}}$ to $\mathcal{S}_K(\widehat{\mathbf{v}})$ for each of 12 edge-

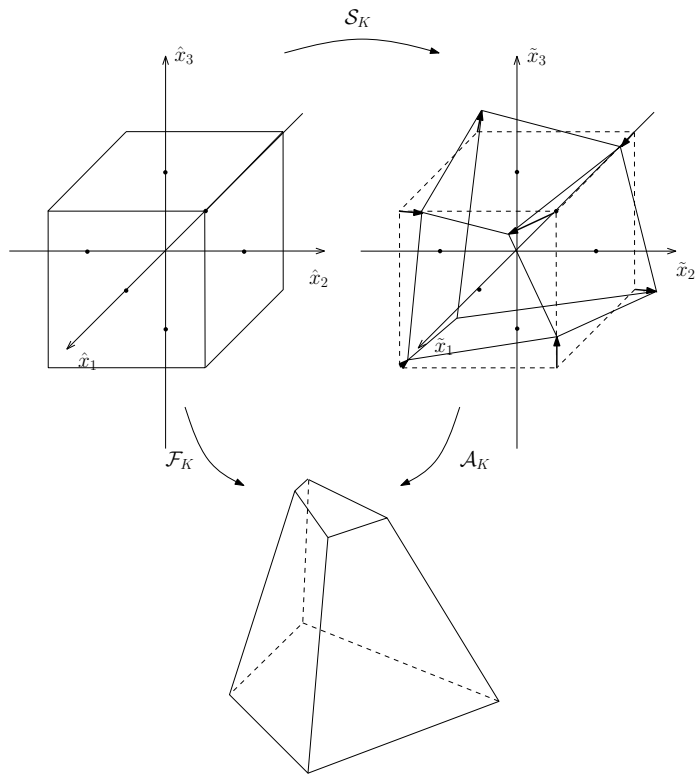

Figure 2.1: A tilinear map $\mathcal{F}_K$ from $\widehat{K}$ to K, a tilinear map $\mathcal{S}_K$ from $\widehat{K}$ to $\widetilde{K}$, and an affine map $\mathcal{A}_K$ from $\widetilde{K}$ to K.

midpoints is given as follows:

$$\widetilde{\mathbf{d}}_{(0,k,l)} = \mathcal{S}_K(0,k,l) - (0,k,l) = kl\widetilde{\mathbf{s}}_1, \quad k,l \in \{1,-1\}, \tag{2.4}$$

$$\widetilde{\mathbf{d}}_{(j,0,l)} = \mathcal{S}_K(j,0,l) - (j,0,l) = jl\widetilde{\mathbf{s}}_2, \quad j,l \in \{1,-1\}, \tag{2.5}$$

$$\widetilde{\mathbf{d}}_{(j,k,0)} = \mathcal{S}_K(j,k,0) - (j,k,0) = jk\widetilde{\mathbf{s}}_3, \quad j,k \in \{1,-1\}. \tag{2.6}$$

The following proposition is immediate.

Proposition 2.2.1. *The three axes* $\{(\widehat{x}_1,0,0) \mid -1 \le \widehat{x}_1 \le 1\}$, $\{(0,\widehat{x}_2,0) \mid -1 \le \widehat{x}_2 \le 1\}$, *and* $\{(0,0,\widehat{x}_3) \mid -1 \le \widehat{x}_3 \le 1\}$ *are invariant under* $\mathcal{S}_K$. *Thus the centers of six faces of* $\widehat{K}$ *are invariant. The face barycenters are given as follows:*

$$\mathbf{c}_j = \frac{1}{|\widetilde{f}_j|}\int_{\widetilde{f}_j} \widetilde{\mathbf{x}}\ \mathrm{d}\widetilde{\mathrm{S}} \qquad j = 1,2,3,4,5,6, \tag{2.7}$$

where $\widetilde{f}_j s$ *are faces of* $\widetilde{K}$.

In [8], the three dimensional nonconforming DSSY element is defined only on parallelogram mesh. In order to construct a three dimensional nonparametric nonconforming finite element space with degrees of freedom which are integral type as in [13], we need to calculate surface integrals on six faces of hexahedron. Let $\widetilde{f}$ be a face of $\widetilde{K}$ such that $\widetilde{f}$ is the image of $\{\widehat{x}_3 = 1\}$ under

the $\mathcal{S}_K$ and $\widetilde{\phi}$ be a polynomial on $\widetilde{K}$,

$$\begin{aligned}
&\int_{\widetilde{f}} \widetilde{\phi}\ \mathrm{d}\widetilde{\mathrm{S}} \\
&= \int_{\widehat{f}} \widehat{\phi} \left\| \frac{\partial \mathcal{S}_K}{\partial \widehat{x}_1}(\widehat{\mathbf{x}}) \times \frac{\partial \mathcal{S}_K}{\partial \widehat{x}_2}(\widehat{\mathbf{x}}) \right\|\ \mathrm{d}\widehat{\mathrm{S}}, \\
&= \int_{-1}^{1}\int_{-1}^{1} \widehat{\phi}\, \|[\widehat{\mathbf{e}}_1 + \widetilde{\mathbf{s}}_2 + \widehat{x}_2(\widetilde{\mathbf{s}}_3 + \widetilde{\mathbf{s}}_4)] \times [\widetilde{\mathbf{e}}_2 + \widetilde{\mathbf{s}}_1 + \widehat{x}_1(\widetilde{\mathbf{s}}_3 + \widetilde{\mathbf{s}}_4)]\|\ d\widehat{x}_1 d\widehat{x}_2, \\
&= \int_{-1}^{1}\int_{-1}^{1} \widehat{\phi} \sqrt{a_0 + a_1\widehat{x}_1 + a_2\widehat{x}_2 + a_3\widehat{x}_1\widehat{x}_2 + a_4\widehat{x}_1^2 + a_5\widehat{x}_2^2}\ d\widehat{x}_1 d\widehat{x}_2,
\end{aligned} \tag{2.8}$$

where, a_j, $j = 0, 1, 2, 3, 4, 5$ are some functions depending on $\widetilde{\mathbf{s}}_k$, $k = 1, 2, 3, 4$ and $\widehat{\mathbf{e}}_k$, $k = 1, 2, 3$ are unit vectors such that k-th component is 1. Since it is hard to calculate the exact integration of (2.8), we have some difficulties to deal with the unisolvency and the error estimations. So we introduce a new approach for hexahedral elements to overcome these drawbacks.

2.2.2 A linearized method for trilinear map

Now, we shall introduce a linearized method for trilinear map. We have already discussed trilinear map can decomposed as

$$\mathcal{F}_K = \mathcal{A}_K \circ \mathcal{S}_K.$$

In order to overcome the difficulty of surface integral, we shall define a new linearized map of $\mathcal{F}_K$. To do this, let us consider the following decomposition of $\widehat{K}$ into five tetrahedrons $\widehat{T}_j$, $j = 1, 2, 3, 4, 5$ as in Figure 2.2 , and denote

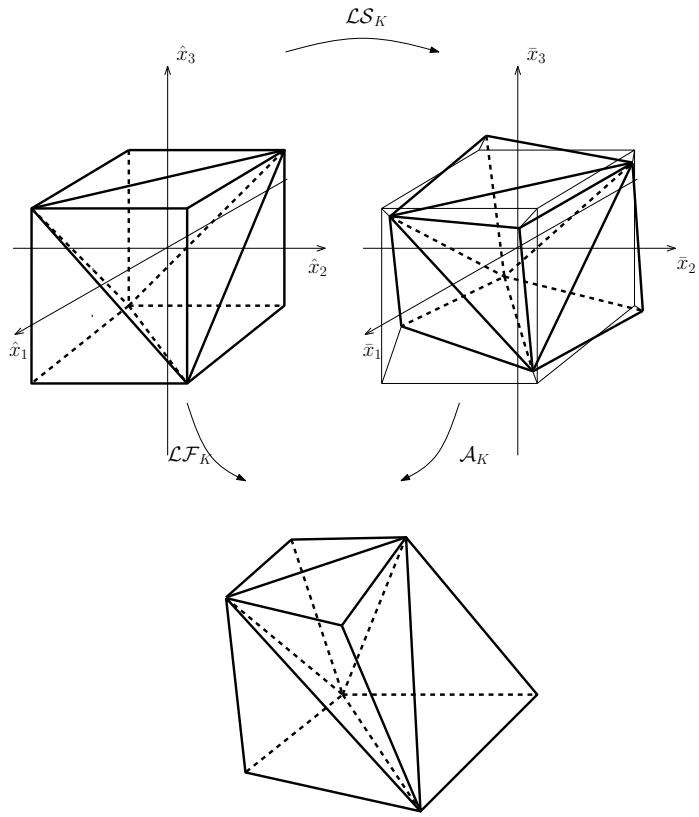

Figure 2.2: A linearized map $\mathcal{LF}_K$ from $\widehat{K}$ to K, a linearized map $\mathcal{LS}_K$ from $\widehat{K}$ to $\bar{K}$, and an affine map $\mathcal{A}_K$ from $\bar{K}$ to K.

the sets of vertices of five tetrahedrons $\widehat{T}_j$ by

$$\begin{aligned}
\rho_1 &= \{\widehat{\mathbf{V}}_{111}, \widehat{\mathbf{V}}_{1-11}, \widehat{\mathbf{V}}_{-111}, \widehat{\mathbf{V}}_{11-1}\} \\
\rho_2 &= \{\widehat{\mathbf{V}}_{-11-1}, \widehat{\mathbf{V}}_{-111}, \widehat{\mathbf{V}}_{-1-1-1}, \widehat{\mathbf{V}}_{11-1}\} \\
\rho_3 &= \{\widehat{\mathbf{V}}_{1-1-1}, \widehat{\mathbf{V}}_{1-11}, \widehat{\mathbf{V}}_{-1-1-1}, \widehat{\mathbf{V}}_{11-1}\} \\
\rho_4 &= \{\widehat{\mathbf{V}}_{-1-11}, \widehat{\mathbf{V}}_{-111}, \widehat{\mathbf{V}}_{1-11}, \widehat{\mathbf{V}}_{-1-1-1}\} \\
\rho_5 &= \{\widehat{\mathbf{V}}_{1-11}, \widehat{\mathbf{V}}_{-111}, \widehat{\mathbf{V}}_{11-1}, \widehat{\mathbf{V}}_{-1-1-1}\}
\end{aligned} \tag{2.9}$$

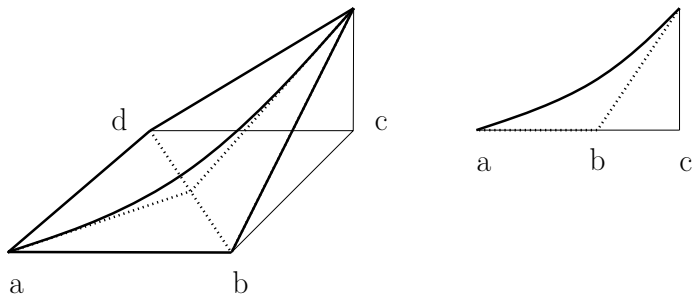

Figure 2.3: A bilinear surface and its linearized surface

Let us define a linearized map $\mathcal{LS}_K$ as follows:

$$\mathcal{LS}_K(\widehat{\mathbf{x}}) = \mathcal{LS}_{T_j}(\widehat{\mathbf{x}}), \qquad \forall\ \widehat{\mathbf{x}} \in \widehat{T}_j, \tag{2.10}$$

where $\mathcal{LS}_{T_m}$ is a affine map such that

$$\mathcal{LS}_{T_m}(\widehat{\mathbf{V}}) = \mathcal{S}_K(\widehat{\mathbf{V}}), \qquad \forall\ \widehat{\mathbf{V}} \in \rho_m, \tag{2.11}$$

for all $m = 1, 2, 3, 4, 5$. For example, the explicit form of $\mathcal{LS}_{T_1}$ are given by

$$\mathcal{LS}_{T_1}(\widehat{\mathbf{x}}) = \mathbf{b}_1 + \mathbf{a}_{1,1}\widehat{x}_1 + \mathbf{a}_{2,1}\widehat{x}_2 + \mathbf{a}_{3,1}\widehat{x}_3, \tag{2.12}$$

where

$$\mathbf{a}_{1,1} = \frac{(\widetilde{\mathbf{V}}_{111} - \widetilde{\mathbf{V}}_{-111})}{2}, \quad \mathbf{a}_{2,1} = \frac{(\widetilde{\mathbf{V}}_{111} - \widetilde{\mathbf{V}}_{1-11})}{2}, \quad \mathbf{a}_{3,1} = \frac{(\widetilde{\mathbf{V}}_{111} - \widetilde{\mathbf{V}}_{11-1})}{2},$$

and

$$\mathbf{b}_1 = \frac{(\widetilde{\mathbf{V}}_{1-11} - \widetilde{\mathbf{V}}_{111} + \widetilde{\mathbf{V}}_{-111} + \widetilde{\mathbf{V}}_{11-1})}{2}.$$

The rest of the explicit form for $\mathcal{LS}_{T_m}$, $m = 2, 3, 4, 5$ can be presented in the similar form.

Let us denote the image of $\widehat{K}$ under the linearized map $\mathcal{LS}_K$ by $\bar{K}$ and

similarly the image of $\widehat{f}_j$ under the linearized map $\mathcal{LS}_K$ is denoted $\bar{f}_j$ for $j = 1, 2, 3, 4, 5, 6$.

Remark 2.2.2. *Note that $\bar{K}$ is same as $\widetilde{K}$ when $\widetilde{K}$ has six flat faces. If $\widetilde{K}$ has a non-flat face and call it $\widetilde{f}$, then the corresponding $\bar{f}$ to $\widetilde{f}$ and $\widetilde{f}$ have the same boundary, but the different shape in their interiors. More precisely, $\bar{f}$ is a union of two flat faces and $\widetilde{f}$ is a bilinear surface with the same boundary. In this sense, we may say that $\bar{K}$ is a linearized domain of $\widetilde{K}$.*

Let us define a linearized map $\mathcal{LF}_K$ for $\mathcal{F}_K$ by

$$\mathcal{LF}_K = \mathcal{A}_K \circ \mathcal{LS}_K.$$

Then, $\mathcal{LF}_K(\widehat{K})$ and $\mathcal{F}_K(\widehat{K})$ have the same 8 vertices and 12 boundary edges. Let $\bar{\phi}(\bar{\mathbf{x}})$ be a polynomial in $\bar{K}$. Then, for any face $\bar{f}$ of $\bar{K}$,

$$\int_{\bar{f}} \bar{\phi}(\bar{\mathbf{x}})\ d\bar{S} = \int_{\bar{f}_1} \bar{\phi}(\bar{\mathbf{x}})\ d\bar{S} + \int_{\bar{f}_2} \bar{\phi}(\bar{\mathbf{x}})\ d\bar{S}, \tag{2.13}$$

where $\bar{f}_1$ and $\bar{f}_2$ are two triangles whose union is $\bar{f}$. For $\bar{f}_1$ and $\bar{f}_2$, let $\mathcal{LS}_{T_{m_j}}$, $j = 1, 2$ be affine maps such that $\bar{f}_j = \mathcal{LS}_{T_{m_j}}(\widehat{f}_j)$, $j = 1, 2$, respectively. Since $\mathcal{LS}_{T_{m_j}}$, $j = 1, 2$ are affine maps and $\bar{\phi}$ is a polynomial, we have

$$\int_{\bar{f}_j} \bar{\phi}(\bar{\mathbf{x}})\ d\bar{S} = \frac{|\bar{f}_j|}{|\widehat{f}_j|} \int_{\widehat{f}_j} \bar{\phi}(\mathcal{LS}_{T_{m_j}}(\widehat{\mathbf{x}}))\ d\widehat{S} \qquad j = 1, 2, \tag{2.14}$$

and so (2.14) can be calculated exactly. Thus the two term on the right hand side of (2.13) can also be exactly calculated. As we mentioned above, the exact surface integral can be easily obtained by $\mathcal{LF}_K$, while it is difficult to exactly calculate the surface integral in the $\mathcal{F}_K$ trilinear map, when we use the linearized map $\mathcal{LF}_K$ instead of $\mathcal{F}_K$ trilinear map. Also, this can be useful

to generalize the nonconforming DSSY element to more general hexahedral mesh.

Definition 2.2.3. *Let us denote six faces* $\{\widehat{x}_1 = 1\}$, $\{\widehat{x}_2 = 1\}$, $\{\widehat{x}_3 = 1\}$, $\{\widehat{x}_1 = -1\}$, $\{\widehat{x}_2 = -1\}$, *and* $\{\widehat{x}_3 = -1\}$ *of* $\widehat{K}$ *by* $\widehat{f}_j$, $j = 1, 2, 3, 4, 5, 6$, *respectively. Similarly,* $\bar{f}_j$ *and* f_j, $j = 1, 2, 3, 4, 5, 6$ *of six faces of* $\bar{K}$ *and* K *are denoted, respectively. Also, let us denote the barycenter of* $\widehat{f}_j$, $\bar{f}_j$, *and* f_j *by* $\widehat{\mathbf{c}}_j$, $\bar{\mathbf{c}}_j$, *and* $\mathbf{c}_j$ *for* $j = 1, 2, 3, 4, 5, 6$, *respectively.*

Assumption 2.2.4. *Let us define a matrix* $D = (\mathbf{d}_1, \mathbf{d}_2, \mathbf{d}_3)^T$, *where* $\mathbf{d}_k = (\bar{\mathbf{c}}_k - \bar{\mathbf{c}}_{k+3})$, *for* $k = 1, 2, 3$. *Then* $det(D) \neq 0$.

Note that Assumption 2.2.4 is geometrically meaningful. Consider the trivial case where $\widetilde{\mathbf{d}}_{jkl} = 0$ for all $j, k, l \in \{-1, 1\}$. Then the octahedron with six vertices $\bar{\mathbf{c}}_j$, $j = 1, 2, 3, 4, 5, 6$ is a dual polyhedron of $\widehat{K}$ as in Figure 2.4a. In this case, clearly $det(D) \neq 0$. Now, suppose that $det(D) = 0$, that is, $\mathbf{d}_1, \mathbf{d}_2$, and $\mathbf{d}_3$ are linearly dependent. This means that the three line segments connecting two opposite barycenters $\bar{\mathbf{c}}_k$, $\bar{\mathbf{c}}_{k+3}$ for $k = 1, 2, 3$ lie on a plane. Actually, this is caused when its dual polyhedron is degenerated into the strange octahedron such as its faced two faces meet each other. For example, consider the case where $\bar{\mathbf{V}}_{jk1} = \widehat{\mathbf{V}}_{jk1}$, for all $j, k \in \{-1, 1\}$ and $\bar{\mathbf{V}}_{jk-1} = \widehat{\mathbf{V}}_{j-k-1}$, for all $j, k \in \{-1, 1\}$ as in Figure 2.5. Then, since $\bar{\mathbf{c}}_k$, $k = 1, 2, 3, 4, 5, 6$ are all in the plane $\{\bar{x}_2 = 0\}$, $det(D) = 0$. In order to avoid the case where the octahedron with six vertices $\bar{\mathbf{c}}_j$, $j = 1, 2, 3, 4, 5, 6$ which is a dual polyhedron of $\bar{K}$ is degenerated into a strange polyhedron, Assumption 2.2.4 is used.

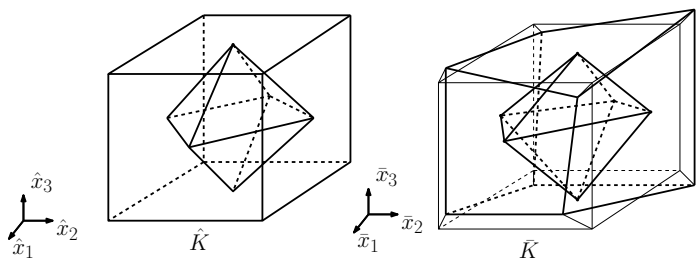

(a) $\widehat{K}$ and its dual polyhedron (b) $\bar{K}$ and its dual polyhedron

Figure 2.4: (a) $\widehat{K}$ and its corresponding dual polyhedron which is a octahedron; (b) $\bar{K}$ and its corresponding dual polyhedron which is a octahedron

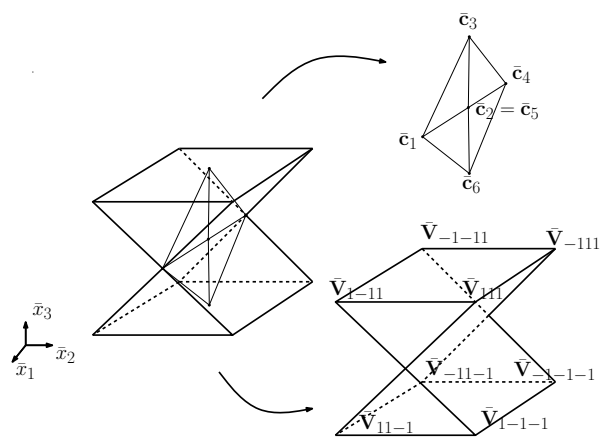

Figure 2.5: In a case of $det(D) = 0$, hexahedron $\bar{K}$ and its corresponding dual polyhedron which is degenerated into a rhombus in a plane.

2.3 Nonparametric nonconforming Finite element space

2.3.1 Nonparametric hexahedral nonconforming DSSY Finite element space

In this section, we introduce three dimensional nonparametric nonconforming finite elements spaces. Firstly, let us define a class of *nonparametric nonconforming elements on the intermediate hexahedrons* $\bar{K}$ with six degrees of freedom as follows.

1. $\bar{K} = \mathcal{LS}_K(\widehat{K})$;
2. $\bar{P}_{\bar{K}} = \mathrm{Span}\{1, \bar{x}_1, \bar{x}_2, \bar{x}_3, \bar{\phi}_1, \bar{\phi}_2\}$;
3. $\bar{\Sigma}_{\bar{K}} = \{$ six mean values over faces of $\bar{K}\}$,

where

$$\begin{aligned} &\bar{\phi}_j = \widehat{\phi}_j \circ \mathcal{LS}_K^{-1}, \qquad j = 1, 2, \text{ and} \\ &\widehat{\phi}_1 = \theta(\widehat{x}_1) - \theta(\widehat{x}_2),\ \widehat{\phi}_2 = \theta(\widehat{x}_1) - \theta(\widehat{x}_3) \text{ for } \theta(t) = t^2 - \frac{5}{3}t^4. \end{aligned} \tag{2.15}$$

Theorem 2.3.1. *For any $K \in \mathcal{T}_h$, $(\bar{K}, \bar{P}_{\bar{K}}, \bar{\Sigma}_{\bar{K}})$ is unisolvent under the Assumption 2.2.4.*

Proof. Let us denote $\bar{x}, \bar{y}, \bar{z}, 1, \bar{\phi}_1$, and $\bar{\phi}_2$ by $\bar{\psi}_j$, $j = 1, 2, 3, 4, 5, 6$, respectively.

Let $A = (a_{jk}) \in M_{6\times 6}(\mathbb{R})$ such that $a_{jk} = \frac{<\bar{\psi}_k, 1>_{\bar{f}_j}}{|\bar{f}_j|}$. Then,

$$A = \begin{pmatrix} \frac{<\bar{x}_1,1>_{\bar{f}_1}}{|\bar{f}_1|} & \frac{<\bar{x}_2,1>_{\bar{f}_1}}{|\bar{f}_1|} & \frac{<\bar{x}_3,1>_{\bar{f}_1}}{|\bar{f}_1|} & 1 & -\frac{2}{3} & -\frac{2}{3} \\ \frac{<\bar{x}_1,1>_{\bar{f}_1}}{|\bar{f}_2|} & \frac{<\bar{x}_2,1>_{\bar{f}_1}}{|\bar{f}_2|} & \frac{<\bar{x}_1,1>_{\bar{f}_2}}{|\bar{f}_2|} & 1 & \frac{2}{3} & 0 \\ \frac{<\bar{x}_1,1>_{\bar{f}_1}}{|\bar{f}_3|} & \frac{<\bar{x}_2,1>_{\bar{f}_1}}{|\bar{f}_3|} & \frac{<\bar{x}_3,1>_{\bar{f}_3}}{|\bar{f}_3|} & 1 & 0 & \frac{2}{3} \\ \frac{<\bar{x}_1,1>_{\bar{f}_1}}{|\bar{f}_4|} & \frac{<\bar{x}_2,1>_{\bar{f}_1}}{|\bar{f}_4|} & \frac{<\bar{x}_3,1>_{\bar{f}_4}}{|\bar{f}_4|} & 1 & -\frac{2}{3} & -\frac{2}{3} \\ \frac{<\bar{x}_1,1>_{\bar{f}_1}}{|\bar{f}_5|} & \frac{<\bar{x}_2,1>_{\bar{f}_1}}{|\bar{f}_5|} & \frac{<\bar{x}_3,1>_{\bar{f}_5}}{|\bar{f}_5|} & 1 & \frac{2}{3} & 0 \\ \frac{<\bar{x}_1,1>_{\bar{f}_1}}{|\bar{f}_6|} & \frac{<\bar{x}_2,1>_{\bar{f}_1}}{|\bar{f}_6|} & \frac{<\bar{x}_3,1>_{\bar{f}_6}}{|\bar{f}_6|} & 1 & 0 & \frac{2}{3} \end{pmatrix}, \tag{2.16}$$

from the fact that

$$\frac{1}{|\bar{f}_j|}\int_{\bar{f}_j} \bar{\phi}_l d\bar{\sigma} = \frac{1}{|\widehat{f}_j|}\int_{\widehat{f}_j} \widehat{\phi}_l d\widehat{\sigma} = \begin{cases} -\frac{2}{3} & \text{if } j = 1, 4 \\ \frac{2}{3} & \text{if } j = 1+l, 4+l \\ 0 & \text{if } j = 4-l, 7-l. \end{cases} \tag{2.17}$$

By some row operations, we have

$$A' = \begin{pmatrix} A_{11} & A_{12} \\ D & 0 \end{pmatrix}, \tag{2.18}$$

where A_{11} and A_{12} are 3×3 minor matrices such that $A_{11} = A(1:3, 1:3)$ and $A_{12} = A(1:3, 4:6)$, respectively, and D is the 3×3 matrix defined in Assumption 2.2.4. Since A_{12} and D are invertible, the matrix A' is also invertible. This completes proof. □

Remark 2.3.2. *Note that the matrix A_{12} is invertible and is same as $A_{22} = A(4:6, 4:6)$ in Theorem 2.3.1. From this fact, we can see that Rannacher-Turek nonconforming finite element similarly can be defined and its unisolvency can be shown as in Theorem 2.3.1. Moreover, we can also define any nonconforming finite element space by choosing $\widehat{\phi}_j$, $j = 1, 2$ to satisfy the con-*

ditions $det(A_{12}) \neq 0$ *and* $A_{12} = A_{22}$.

Since the affine map $\mathcal{A}_K$ preserves the integral values on each face and the unisolvency, it is straightforward to define local basis functions in the physical domain K. Thus a class of *nonparametric nonconforming elements on hexahedrons* K with six degrees of freedom is defined as follows.

1. $K = \mathcal{LF}_K(\widehat{K})$;
2. $\mathcal{NC}_K = \text{Span}\{\psi \mid \psi = \bar{\psi} \circ \mathcal{A}_K^{-1},\ \bar{\psi} \in \bar{P}_{\bar{K}}\}$;
3. $\Sigma_K = \{\text{six mean values over faces of } K\}$.

Let $\phi_j = \bar{\phi}_j \circ \mathcal{A}_K^{-1}$, $j = 1, 2$. Then, ϕ_j, $j = 1, 2$ are piecewise fourth order polynomial functions in general. But if K is a parallelogram then these functions can be represented by whole fourth order polynomial functions in K and are same as the parametric DSSY basis functions in [8]. Thus the nonparametric DSSY element we introduced in the above can be interpreted as a generalization of the three dimensional DSSY nonconforming finite element introduced in [8]. We now define global nonparametric DSSY element spaces as follows:

$$\begin{aligned}\mathcal{NC}^h = \{&v_h \in L^2(\Omega) \mid v_h|_K \in \mathcal{NC}_K\ \forall K \in \mathcal{T}_h \text{ and} \\ &< v_h|_K - v_h|_{K'}, 1 >_{K \cap K'} = 0 \text{ for any adjacent two } K, K' \in \mathcal{T}_h\},\end{aligned}$$

$$\mathcal{NC}_0^h = \{v_h \in \mathcal{NC}_h^{np} \mid v_h \text{ is zero at the centroid of each } f \in \mathcal{F}_h \cap \partial\Omega\}.$$

2.3.2 An interpretation as a tetrahedral macro-element

In this subsection, we discuss that the proposed nonparametric DSSY element on hexahedral grid can be interpreted as tetrahedral macro-element.

Consider a reference tetrahedron domain $\check{T}$ surrounded by four plane $\{\check{x}_1 = 0\}$, $\{\check{x}_2 = 0\}$, $\{\check{x}_3 = 0\}$ and $\{\check{x}_1 + \check{x}_2 + \check{x}_2 = 1\}$ as in Figure 2.6. Let us define

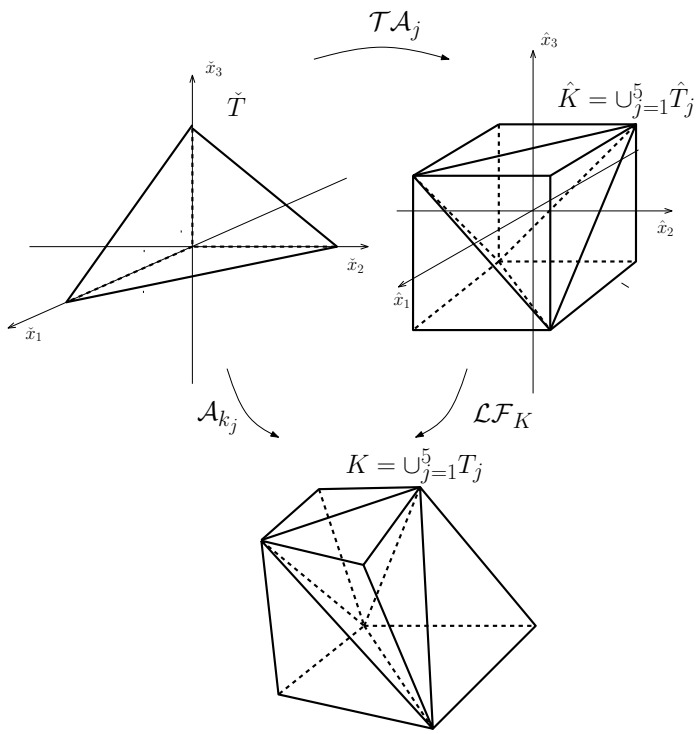

Figure 2.6: An affine map $\mathcal{TA}_j$ from $\check{T}$ to $\widehat{T}_j$, an affine map $\mathcal{A}_{K_j}$ from $\check{T}$ to T_j for $j = 1, 2, 3, 4, 5$ and $\mathcal{LF}_K$ from $\widehat{K}$ to K.

five affine maps such that

$$\mathcal{TA}_j(\check{T}) = \widehat{T}_j, \qquad j = 1, 2, 3, 4, 5. \tag{2.19}$$

Then, $(K, \mathcal{NC}_K, \Sigma_K)$ can be written as

1. $K = \bigcup_{j=1}^{5} \mathcal{A}_{K_j}(\check{T})$;
2. $\mathcal{NC}_K = P_1(K) \bigoplus \text{Span}\{\phi_l \mid \phi_l|_{T_j} = \check{\phi}_{l,j} \circ \mathcal{A}_{K_j}^{-1}, l = 1, 2, j = 1, 2, 3, 4, 5\}$;
3. $\Sigma_K = \{\text{six mean values over faces of } K\}$,

where $\check{\phi}_{l,j}$ is a polynomial in $\check{T}$ such that $\check{\phi}_{l,j}(\check{\mathbf{x}}) = \widehat{\phi}_l \circ \mathcal{TA}_j^{-1}(\widehat{\mathbf{x}})$ for $l = 1, 2$ and $j = 1, 2, 3, 4, 5$. If we consider K as the tetrahedral macro-element which

is a union of five tetrahedron T_j,$j = 1, 2, 3, 4, 5$ and the basis functions on K are given by piecewise polynomials which belong to $\mathcal{NC}_K$. $(K, \mathcal{NC}_K, \Sigma_K)$ can be regarded as a tetrahedral macro-element from the above interpretation.

2.3.3 A priori error estimation and a new finite element space

In this subsection, we need some notations before we discuss the error estimation. Let $\Omega = \cup_j \Omega_j$, where Ω_j is a hexahedron element which has numbering j. Also, let us denote

$$\Gamma_{jk} = \Gamma_{kj} = \partial\Omega_j \cap \partial\Omega_k, \quad \Gamma_j = \partial\Omega \cap \partial\Omega_j, \tag{2.20}$$

Consider the following the second Strang lemma :

Lemma 2.3.3. *If $u_h \in \mathcal{NC}_0^h$ is the solution of problem and $u \in H_0^1(\Omega)$ the solution problem, then*

$$||u - u_h||_{1,h} \leq C \left\{ \inf_{v \in NC_0^h} ||u - v||_{1,h} + \sup_{w \in NC_0^h} \frac{|a_h(u, w) - F_h(w)|}{||w||_{1,h}} \right\}. \tag{2.21}$$

Since the unisolvency of $\mathcal{NC}_0^h$ holds,

$$\inf_{v \in NC_0^h} ||u - v||_{1,h} \leq Ch||u||_2. \tag{2.22}$$

The remaining part is the following consistency error

$$\sup_{w \in NC_0^h} \frac{|a_h(u, w) - F_h(w)|}{||w||_{1,h}}. \tag{2.23}$$

Note that

$$a_h(u, w) - F_h(w) = \sum_j \left\langle \frac{\partial u}{\partial \nu}, w \right\rangle_{\partial\Omega_j \setminus \Gamma_j}. \tag{2.24}$$

Now, Define a projection $\Pi : H^2(\Omega) \cap H_0^1(\Omega) \to \mathcal{NC}_0^h$ and $P_0 : H^1(\Omega) \to \Lambda^h$, by

$$\begin{aligned} \langle v - \Pi v, 1 \rangle_\Gamma &= 0, \qquad \forall \Gamma, \\ \left\langle \frac{\partial v}{\partial \nu} - P_0 \frac{\partial v}{\partial \nu}, z \right\rangle_\Gamma &= 0, \qquad z \in P_0(\Gamma), \forall \Gamma \end{aligned} \tag{2.25}$$

where, $\Lambda^h = \{\lambda \mid \lambda_{jk} = tr_{\Gamma_{jk}}(\lambda|_{\Omega_j}) \in P_0(\gamma_{jk});\ \lambda_{jk} + \lambda_{kj} = 0; \lambda_j = tr_{\Gamma_j}(\lambda|\Omega_j) \in P_0(\Gamma_j)\}$

From standard polynomial approximation theory, we have

$$\left(\sum_j \left| \frac{\partial v}{\partial \nu} - P_0 \frac{\partial v}{\partial \nu} \right|_j^2 \right)^{\frac{1}{2}} \leq C h^{\frac{1}{2}} ||v||_2 \tag{2.26}$$

In order to bound the consistency error part, we need the following useful orthogonality :

$$\left\langle P_0 \frac{\partial u}{\partial \nu}, w_j \right\rangle_{\Gamma_{jk}} + \left\langle P_0 \frac{\partial u}{\partial \nu}, w_k \right\rangle_{\Gamma_{kj}} = \left\langle P_0 \frac{\partial u}{\partial \nu}, w_j - w_k \right\rangle_{\Gamma_{jk}} = 0 \tag{2.27}$$

This is from the fact that the degrees of freedom for $\mathcal{NC}_0^h$ are defined by the integral values at the interfaces and $P_0 \frac{\partial u}{\partial \nu}$ is constant on Γ_{jk}. Thus, it follows that

$$\sum_j \left\langle \frac{\partial u}{\partial \nu}, w \right\rangle_{\Omega_j \setminus \Gamma_j} = \sum_j \left\langle \frac{\partial u}{\partial \nu} - P_0 \frac{\partial u}{\partial \nu}, w - m \right\rangle_{\Omega_j \setminus \Gamma_j} \tag{2.28}$$

for some piecewise constant function m which is a locally average value of w over Ω_j. Thus we have

$$\left| \sum_j \left\langle \frac{\partial u}{\partial \nu} - P_0 \frac{\partial u}{\partial \nu}, w - m \right\rangle_{\Omega_j \setminus \Gamma_j} \right| \leq C h ||u||_2 ||w||_{1,h} \tag{2.29}$$

by (2.26). Now, consider the case in which hexahedrons have a non-flat surface. In this case, Since $\frac{\partial u}{\partial \nu}$ is discontinuous functions we can not use (2.26). It can cause the reduction of convergence order. In order to solve the weak point, we introduce a new finite element space which has 12 basis and degrees of freedom. Let $\psi_j = \widehat{\psi}_j \circ \mathcal{LF}_K^{-1}$, $j = 1, 2, ..., 8$, where

$$\begin{aligned} &\widehat{\psi}_1 = \theta(\widehat{x}_1) - \theta(\widehat{x}_2), \quad \widehat{\psi}_2 = \theta(\widehat{x}_1) - \theta(\widehat{x}_3), \\ &\widehat{\psi}_3 = \widehat{x}_2\widehat{x}_3, \quad \widehat{\psi}_4 = \widehat{x}_3\widehat{x}_1, \quad \widehat{\psi}_5 = \widehat{x}_1\widehat{x}_2, \\ &\widehat{\psi}_6 = \widehat{x}_1^2\widehat{x}_3, \quad \widehat{\psi}_7 = \widehat{x}_2^2\widehat{x}_1, \quad \widehat{\psi}_8 = \widehat{x}_3^2\widehat{x}_2 \end{aligned} \tag{2.30}$$

for $\theta(t) = t^2 - \frac{5}{3}t^4$.

1. $K = \mathcal{LF}_K(\widehat{K})$;
2. $\mathcal{NC}_K = P_1(K) \bigoplus \mathrm{Span}\{\psi_j\}_{j=1}^8$;
3. $\Sigma_K = \{\text{mean values over 12 triangles on 6 faces of } K\}$.

Let $w \in \mathcal{NC}_0^h$. For any $\Gamma_{jk} = \Omega_j \cap \Omega_k$, let $\Gamma_{jk,1}$ and $\Gamma_{jk,2}$ are two triangles such that $\Gamma_{jk} = \Gamma_{jk,1} \cap \Gamma_{jk,2}$. Then, since $P_0\frac{\partial u}{\partial \nu}$ is a constant on each $\Gamma_{jk,1}$ and $\Gamma_{jk,2}$, and the mean value of w is continuous on each two triangles $\Gamma_{jk,1}$ and $\Gamma_{jk,2}$, we have

$$\begin{aligned} &\left\langle P_0\frac{\partial u}{\partial \nu}, w_j \right\rangle_{\Gamma_{jk}} + \left\langle P_0\frac{\partial u}{\partial \nu}, w_k \right\rangle_{\Gamma_{kj}} \\ &= \left\langle P_0\frac{\partial u}{\partial \nu}, w_j \right\rangle_{\Gamma_{jk,1}} + \left\langle P_0\frac{\partial u}{\partial \nu}, w_j \right\rangle_{\Gamma_{jk,2}} + \left\langle P_0\frac{\partial u}{\partial \nu}, w_k \right\rangle_{\Gamma_{kj,1}} + \left\langle P_0\frac{\partial u}{\partial \nu}, w_k \right\rangle_{\Gamma_{kj,2}} \\ &= \left\langle P_0\frac{\partial u}{\partial \nu}, w_j - w_k \right\rangle_{\Gamma_{jk,1}} + \left\langle P_0\frac{\partial u}{\partial \nu}, w_j - w_k \right\rangle_{\Gamma_{jk,2}} \\ &= 0. \end{aligned} \tag{2.31}$$

Thus, the finite element space with locally twelve basis functions can be used to obtain the optimal convergence order for the non-flat case instead of the finite element with locally six basis functions.

2.4 Numerical results

In this section, we perform numerical experiments for a simple elliptic problem with homogeneous Dirichlet boundary condition:

$$\begin{aligned} -\Delta u &= f \qquad \text{in } \Omega, \\ u &= 0 \qquad \text{on } \partial\Omega, \end{aligned}$$

on the domain $\Omega = (0,1)^3$. The source function f is given so that the exact solution is

$$u(\mathbf{x}) = x_1^2(x_1-1)x_2(x_2-1)(2x_2-1)x_3(x_3-1)(2x_3-1).$$

At first, let us denote the two nonparametric finite element spaces with locally six basis functions and twelve basis functions by $\mathcal{NC}_{0,6}^h$ and $\mathcal{NC}_{0,12}^h$, respectively. We test the above problem for the three types of mesh including uniform cube mesh, trapezoidal mesh, and randomly perturbed mesh as in Figure 2.7a, Figure 2.7b, and Figure 2.8. Table 2.1, Table 2.2, and Table 2.3 the numerical results for $\mathcal{NC}_{0,6}^h$. We can see that the optimal convergence is obtained for flat meshes including cube mesh, trapezoidal mesh, but randomly perturbed mesh. From this result, we can see that $\mathcal{NC}_{0,6}^h$ can not be work for non-flat mesh. However, for the case of $\mathcal{NC}_{0,12}^h$, we have the results Table 2.4, Table 2.5, and Table 2.6, which shows that all the cases work well.

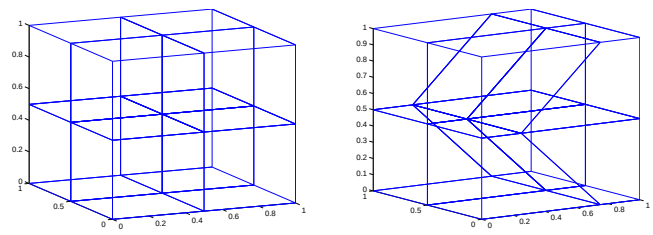

(a) Uniform hexahedron mesh (b) Hexahedron with two trapezoidal mesh

Figure 2.7: (a) Uniform hexahedron mesh consisting of cubes; (b) Hexahedron with two trapezoidal mesh

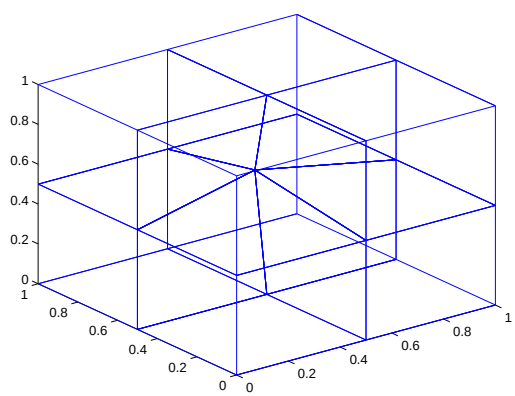

Figure 2.8: A mesh decomposition such that interior points are randomly perturbed from the uniform mesh

h	$\|\|u-u_h\|\|_{0,\Omega}$	ratio	$\|\|u-u_h\|\|_{1,h}$	ratio
1/2	0.3831E-03	-	0.4424E-02	-
1/4	0.1524E-03	1.33	0.3209E-02	0.46
1/8	0.4089E-04	1.90	0.1679E-02	0.93
1/16	0.1040E-04	1.98	0.8477E-03	0.99
1/32	0.2610E-05	1.99	0.4249E-03	1.00
1/64	0.6530E-06	2.00	0.2125E-03	1.00

Table 2.1: Computational results of $\mathcal{NC}^h_{0,6}$ for the Poisson problem for the uniform mesh.

h	$\|\|u-u_h\|\|_{0,\Omega}$	ratio	$\|\|u-u_h\|\|_{1,h}$	ratio
1/2	0.4098E-03	-	0.4423E-02	-
1/4	0.1462E-03	1.49	0.3172E-02	0.48
1/8	0.4463E-04	1.71	0.1739E-02	0.87
1/16	0.1204E-04	1.89	0.8919E-03	0.96
1/32	0.3152E-05	1.93	0.4503E-03	0.98
1/64	0.8078E-06	1.96	0.2262E-03	0.99

Table 2.2: Computational results of $\mathcal{NC}^h_{0,6}$ for the Poisson problem for the hexahedron with two trapezoidal mesh.

h	$\|\|u-u_h\|\|_{0,\Omega}$	ratio	$\|\|u-u_h\|\|_{1,h}$	ratio
1/2	0.3836E-03	-	0.4427E-02	-
1/4	0.1887E-03	1.02	0.3462E-02	0.35
1/8	0.7471E-04	1.34	0.2097E-02	0.72
1/16	0.3077E-04	1.28	0.1255E-02	0.74
1/32	0.1701E-04	0.86	0.8394E-03	0.58
1/64	0.1237E-04	0.46	0.6876E-03	0.29

Table 2.3: Computational results of $\mathcal{NC}^h_{0,6}$ for the Poisson problem for the random mesh.

h	$\|\|u-u_h\|\|_{0,\Omega}$	ratio	$\|\|u-u_h\|\|_{1,h}$	ratio
1/2	0.3891E-03	-	0.4480E-02	-
1/4	0.1338E-03	1.54	0.2803E-02	0.68
1/8	0.3221E-04	2.05	0.1323E-02	1.08
1/16	0.8085E-05	1.99	0.6579E-03	1.01
1/32	0.2025E-05	2.00	0.3285E-03	1.00
1/64	0.5065E-06	2.00	0.1642E-03	1.00

Table 2.4: Computational results of $\mathcal{NC}^h_{0,12}$ for the Poisson problem for the uniform mesh.

h	$\|\|u-u_h\|\|_{0,\Omega}$	ratio	$\|\|u-u_h\|\|_{1,h}$	ratio
1/2	0.4046E-03	-	0.4490E-02	-
1/4	0.1241E-03	1.70	0.2797E-02	0.68
1/8	0.3497E-04	1.83	0.1404E-02	0.99
1/16	0.9145E-05	1.94	0.7076E-03	0.99
1/32	0.2327E-05	1.97	0.3550E-03	1.00
1/64	0.5861E-06	1.99	0.1778E-03	1.00

Table 2.5: Computational results of $\mathcal{NC}^h_{0,12}$ for the Poisson problem for the hexahedron with two trapezoidal mesh.

h	$\|\|u-u_h\|\|_{0,\Omega}$	ratio	$\|\|u-u_h\|\|_{1,h}$	ratio
1/2	0.3889E-03	-	0.4488E-02	-
1/4	0.1371E-03	1.50	0.2855E-02	0.65
1/8	0.3425E-04	2.00	0.1366E-02	1.06
1/16	0.8683E-05	1.98	0.6828E-03	1.00
1/32	0.2168E-05	2.00	0.3411E-03	1.00
1/64	0.5419E-06	2.00	0.1706E-03	1.00

Table 2.6: Computational results of $\mathcal{NC}^h_{0,12}$ for the Poisson problem for the random mesh.

Chapter 3

A nonparametric DSSY element with maximal inf-sup constant

3.1 Introduction

In the paper, we introduce a new nonparametric nonconforming quadrilateral finite element. When fluid mechanics problems are dealt with, simplest and lowest order nonconforming finite elements are used for the stability of its numerical solution rather than conforming finite element in many cases. These lowest order nonconforming finite elements have locally four basis functions including P_1. The special basis function except for linear polynomials are can be chosen in many other ways, for instance [4, 8, 10, 22]. In spite of the freedom to choose the additional basis function, a natural question occurs : what is the optimal choice ? In [11], Jeon, Nam, and Sheen provided an answer for the question. The answer is to choose the extra function such that inf-sup constant for Stokes problem is maximized. The extra basis function of Rannacher

and Turek element[22] is $l_1(x,y)^2 - l_2(x,y)^2$, where $l_1(x,y)$ and $l_2(x,y)$ are linear polynomials such that $l_1 = 0$ and $l_2 = 0$ are two lines equations passing through midpoints of faced edges on quadrilateral. And clearly this is in P_2. Instead of this function, one may choose another extra polynomial in P_2 which make the inf-sup constant maximum. Since the minimal value of H_1-seminorm of velocity space in each element implies the maximal inf-sup constant for the Stokes problem, a minimization problem is solved to find the basis function.

Naturally we may think whether it is possible to apply this idea to DSSY element [8] as well. The aim of the paper is to provide an answer of the curiosity. In order to apply the same idea to DSSY element we have to use the nonparametric DSSY element introduced in [13], instead of the parametric version. Because for any quadrilateral triangulation we need to construct a finite element which has only four local basis and optimal convergence property. The nonparametric DSSY element lies between P_1 and P_4 spaces. Contrast to [11], DSSY element have to satisfies *the mean value property* which means that the midpoint value and the mean value on each interface agree. Thus we use the restricted subspace $P_{4,mvp}$ of P_4 which satisfies the mean value property to solve the constrained minimization problem. Similar to [11] it can be interpreted as an improved nonparametric DSSY element.

For historical information about the nonconforming finite element, we refer the readers to [1, 7, 8, 9, 10, 16, 20, 22].

The paper is organized as follows. Notations and basic concepts used in whole paper are presented in Section 2. In section 3, nonparametric quadrilateral element with the maximal inf-sup constant is introduced and its properties are deal with. Next, numerical scheme for finding basis functions are introduced in section 4. Finally, numerical results for the Stokes equations are presented to compare the proposed finite element and the nonparametric

DSSY element.

3.2 Notations and preliminaries

Let Ω be a simply connected polygonal domain in $\mathbb{R}^2$ and $(\mathcal{T}_h)_{h>0}$ be a family of shape regular quasi uniform quadrilateral triangulations of Ω with $\max_{K\in\mathcal{T}_h} diam(K) = h$. Let us denote by $\mathcal{E}_h$ the set of all edge in $\mathcal{T}_h$. For an element $K \in \mathcal{T}_h$ we denote four vertices of K by $\mathbf{v}_j$ for $j = 1, 2, 3, 4$ and also denote an edge passing through $\mathbf{v}_{j-1}$ and $\mathbf{v}_j$ by e_j and a midpoint of e_j by $\mathbf{m}_j$ for $j = 1, 2, 3, 4$ ($\mathbf{v}_0 := \mathbf{v}_4$).

For a set $D \subset \mathbb{R}^2$ we denote by $H^s(D)$ the usual Sobolev space with norm $||\cdot||_{s,D}$ and seminorm $|\cdot|_{s,D}$ for $n = 0, 1$. $H_0^s(D)$ is the sobolev space consisting of functions of $H^s(D)$ whose traces vanish up to order $s-1$ on ∂D. The space of square integrable with zero mean value is denoted by $L_0^2(D)$.

The L^2 inner product over two dimensional domain D is denoted by $(\cdot,\cdot)_D$. In particular if D is one dimensional set, then we denote L^2 inner product by $< \cdot, \cdot >_D$. For simplicity if $D = \Omega$, then we set $(\cdot,\cdot) := (\cdot,\cdot)_\Omega$ and $< \cdot, \cdot >:=< \cdot, \cdot >_{\partial\Omega}$. The following standard norms will be adopted:

$$|\mathbf{v}|_{1,h} = \left(\sum_K ||\nabla\, \mathbf{v}||_{0,K}^2\right)^{\frac{1}{2}}, \quad ||\mathbf{v}||_{1,h} = (||\mathbf{v}||_{0,\Omega}^2 + |\mathbf{v}|_{1,h}^2)^{\frac{1}{2}}$$

for all $\mathbf{v} \in [H_0^1(\Omega)]^2 + [\mathcal{NC}_h]^2$,

where $\mathcal{NC}_h$ is a nonconforming finite element space.

In this paper, we call the following conditions *the mean value conditions*. For $K \in \mathcal{T}_h$ and $v \in H^1(K)$

$$v(\mathbf{m}_j) = \frac{< v, 1 >_{e_j}}{|e_j|}, \qquad j = 1, 2, 3, 4. \tag{3.1}$$

In fact, these conditions are the essential properties of DSSY element [8], [13].

Let us recall the nonparametric DSSY element [13]. For any $K \in \mathcal{T}_h$

$$\mathcal{NC}_K^{DSSY} = \text{Span}\{1, x, y, \mu(x, y; \widetilde{c})\},$$

where

$$\mu(x, y; \widetilde{c}) = -\frac{5}{3} l_1(x, y) l_2(x, y) q(x, y; \widetilde{c})$$

and $l_1(x, y)$, $l_2(x, y)$ are two linear polynomials and $q(x, y)$ is a quadratic polynomial such that lines $l_1(x, y) = 0$ and $l_2(x, y) = 0$ are passing through $\mathbf{v}_1$, $\mathbf{v}_3$ and $\mathbf{v}_2$, $\mathbf{v}_4$, respectively, and $q(x, y; \widetilde{c}) = 0$ is an ellipse which is determined to satisfy the mean value property (3.1) for μ.

$\mathcal{NC}_K^{DSSY}$ is a local nonparametric DSSY element. We can define global nonparametric DSSY element spaces as follows

$$\mathcal{NC}_h^{np} = \{v_h \in L^2(\Omega) \mid v_h|_K \in \mathcal{NC}_K^{DSSY} \text{ for } K \in \mathcal{T}_h, v_h \text{ is continuous at the midpoint of each } e \in \mathcal{E}_h\},$$

$$\mathcal{NC}_{h,0}^{np} = \{v_h \in \mathcal{NC}_h^{np} \mid v_h \text{ is zero at the midpoint of each } e \in \mathcal{E}_h \cap \partial\Omega\}.$$

Let us consider the Stokes equations :

$$\begin{aligned} -\Delta \mathbf{u} + \nabla p &= \mathbf{f} \qquad \text{in } \Omega, \\ \nabla \cdot \mathbf{u} &= 0 \qquad \text{in } \Omega, \\ \mathbf{u} &= 0 \qquad \text{on } \partial\Omega, \end{aligned} \tag{3.2}$$

where $\mathbf{f} \in [L^2(\Omega)]^2$. And the variational problem of (3.2) is to find $(\mathbf{u}, p) \in$

$[H_0^1(\Omega)]^2 \times L_0^2(\Omega)$

$$\begin{aligned} (\nabla \mathbf{u}, \nabla \mathbf{v}) - (p, \nabla \cdot \mathbf{v}) &= (\mathbf{f}, \mathbf{v}) \qquad \forall \mathbf{v} \in [H_0^1(\Omega)]^2, \\ (\nabla \cdot \mathbf{u}, q) &= 0 \qquad \forall q \in L_0^2(\Omega). \end{aligned} \tag{3.3}$$

We consider a pair of nonconforming finite element spaces $[\mathcal{NC}_{h,0}^{np}]^2 \times P_{h,0}$, where

$$P_{h,0} = \{q \in L^2(\Omega) \mid q|_K \in P_0(K) \ \forall K \in \mathcal{T}_h \text{ and } \int_\Omega q d\mathbf{x} = 0\}.$$

If we use the nonconforming finite element spaces $[\mathcal{NC}_{h,0}^{np}]^2 \times P_{h,0}$, then the discretized problem of (3.3) is given as follows : Find $(\mathbf{u}_h, p_h) \in [\mathcal{NC}_{h,0}^{np}]^2 \times P_{h,0}$

$$\begin{aligned} \sum_{K \in \mathcal{T}_h} (\nabla_h \mathbf{u}_h, \nabla_h \mathbf{v}_h) - \sum_{K \in \mathcal{T}_h} (p_h, \nabla_h \cdot \mathbf{v}_h) &= (\mathbf{f}, \mathbf{v}_h) \qquad \forall \mathbf{v}_h \in [\mathcal{NC}_{h,0}^{np}]^2, \\ \sum_{K \in \mathcal{T}_h} (\nabla_h \cdot \mathbf{u}_h, q_h) &= 0 \qquad \forall q_h \in P_{h,0}, \end{aligned} \tag{3.4}$$

where ∇_h and $\nabla_h \cdot$ are discrete gradient and divergence operator, respectively.

As shown in [5], [13], we know that the discrete inf-sup condition holds for $[\mathcal{NC}_{h,0}^{np}]^2 \times P_{h,0}$, that is, there exists a positive constant β^{DSSY} such that

$$0 < \beta^{DSSY} = \inf_{q \in P_{h,0}} \sup_{\mathbf{v} \in [\mathcal{NC}_{h,0}^{np}]^2} \frac{(\nabla_h \cdot \mathbf{v}, q)}{|\mathbf{v}|_{1,h} ||q||_{0,\Omega}}. \tag{3.5}$$

Similar to [11], our purpose is to find a new quadrilateral element which is improved to have a bigger inf-sup constant than β^{DSSY}. To make inf-sup constant bigger, we have to construct a new finite element such that the values of H^1-seminorm of the velocity space become as small as possible. Since $\mathcal{NC}_K^{DSSY} \subset P_4(K)$, our strategy is to construct a new finite element space $\mathcal{NC}_K^{new} \subset P_4(K)$ satisfying the constrained minimization condition: if

$v \in \mathcal{NC}_K^{new}$, then

$$|v|_{1,K}^2 = \min\{|w|_{1,K}^2 \mid w(\mathbf{m}_j) = v(\mathbf{m}_j) \text{ and } w(\mathbf{m}_j) = \frac{< w, 1 >_{e_j}}{|e_j|},\ j = 1, 2, 3, 4, \text{ for } w \in P_4(K)\}.$$

This means that $\mathcal{NC}_K^{new}$ will be constructed such that its basis functions are polynomials which has the minimal value of H^1-seminorm among the polynomials satisfying the mean value property and having the same midpoint values. In the next section, we shall construct a new finite element by using this concept.

3.3 New nonparametric DSSY quadrilateral element with maximal inf-sup constant

Let us define

$$P_{4,mvp}(K) = \{v \in P_4(K) \mid v(\mathbf{m}_j) = \frac{< v, 1 >_{e_j}}{|e_j|},\ j = 1, 2, 3, 4\}.$$

For any $\mathbf{c} = (c_1, c_2, c_3, c_4)^T \in \mathbb{R}^4$, we also define

$$P_{4,mvp,\mathbf{c}}(K) = \{v \in P_{4,mvp}(K) \mid v(\mathbf{m}_j) = c_j,\ j = 1, 2, 3, 4\}.$$

Here, we should check that the dimension of $P_{4,mvp}(K)$. Since the dimension of $P_4(K)$ is 15 and $P_{4,mvp}(K)$ is a restricted subspace of $P_4(K)$ by four mean value conditions, we know that $\dim(P_{4,mvp}(K)) \geq 11$. From [13], we can see that $P_{4,mvp}(K) = \mathcal{NC}_K^{DSSY} \oplus P_{4,mvp,\mathbf{0}}(K)$. We shall show that $\dim(P_{4,mvp}) = 11$ by proving $\dim(P_{4,mvp,\mathbf{0}}(K)) = 7$ in the following lemma.

Lemma 3.3.1. *For any $K \in \mathcal{T}_h$, $P_{4,mvp,\mathbf{0}}(K)$ has 7 dimension. Therefore for any $\mathbf{c} \in \mathbb{R}^4$ $P_{4,mvp,\mathbf{c}}(K)$ has 7 dimension and $P_{4,mvp}(K)$ has 11 dimension.*

Proof. As in [2], we can consider the trace operator γ from $P_4(K)$ to $\prod_{l=1}^4 P_4(e_l)$. We know that $\dim(P_4(K)) = 15$ and $\ker(\gamma) = \text{Span}\{l_1 l_2 l_3 l_4\}$, where $l_j = 0$ is line equation of e_j for $j = 1, 2, 3, 4$. Thus $\dim(Im(\gamma)) = 14$. Since $\dim(\prod_{l=1}^4 P_4(e_l)) = 20$, if we impose independent 6 compatibility conditions on $\prod_{l=1}^4 P_4(e_l)$ then we can recover the range space of γ from $\prod_{l=1}^4 P_4(e_l)$. These 6 compatibility conditions can be obtained from continuity conditions at 6 points of intersection produced by four lines $l_j = 0$ for $j = 1, 2, 3, 4$. Surely when the faced two edges each other are parallel, the intersection points are four or five. In this case we use the condition that the leading coefficients of the polynomial traces on two opposite edges must coincide as in ([2],p72). Now let us consider a restricted trace operator γ' from $P_{4,mvp,\mathbf{0}}(K)$ to $\prod_{l=1}^4 P_4(e_l)$ where the domain $P_4(K)$ are restricted to $P_{4,mvp,\mathbf{0}}(K)$. Since $l_1 l_2 l_3 l_4 \in P_{4,mvp,\mathbf{0}}(K)$, $\ker(\gamma) = \ker(\gamma')$ and so $\dim(\ker(\gamma')) = 1$. Also $Im(\gamma')$ can be recovered by 14 conditions (6 compatibility conditions, 4 mean value conditions, and 4 conditions of having zero values at midpoints of four edges of K) from $\prod_{l=1}^4 P_4(e_l)$. We can easily check these 14 conditions are independent. Therefore the dimension of range of γ' is 6. Since $\dim(P_{4,mvp,\mathbf{0}}(K)) = \dim(Ker(\gamma')) + \dim(Im(\gamma'))$, we can see $\dim(P_{4,mvp,\mathbf{0}}(K)) = 7$. Moreover we can see that $\dim(P_{4,mvp}(K)) = 11$ from $\dim(\mathcal{NC}_K^{DSSY}) = 4$. And $P_{4,mvp,\mathbf{c}}(K) = \text{Span}\{\phi + q \mid \phi \in \mathcal{NC}_K^{DSSY},\ \phi(\mathbf{m}_l) = c_l\ \forall\ l,\ \text{and}\ q \in P_{4,mvp,\mathbf{0}}(K)\}$ implies $\dim(P_{4,mvp,\mathbf{c}}(K)) = 7$. □

Remark 3.3.2. *Lemma 3.3.1 means that the mean value conditions give independent 4 constraints to determine basis functions for all $K \in \mathcal{T}_h$, that is, $dim(P_{4,mvp}(K)) = 11$. For any polynomial space $P_n(K)$ for $n \geq 4$, one can construct $P_{n,mvp}(K)$ in the same manner. Since the mean value conditions*

also give independent 4 constraints for $P_n(K)$ *where* $n \geq 4$, $dim(P_{n,mvp}(K)) = dim(P_n) - 4 = \frac{(n+1)(n+2)}{2} - 4$ *holds.*

As in [11], we consider the constrained minimization problem: For given $\mathbf{c} \in \mathbb{R}^4$, find $v \in P_{4,mvp}(K)$ such that

$$|v|^2_{1,K} = \min_{w \in P_{4,mvp,\mathbf{c}}(K)} |w|^2_{1,K} \qquad \text{subject to} \;\; v(\mathbf{m}_j) = c_j, \quad j = 1,2,3,4. \tag{3.6}$$

The problem (3.6) can be equivalently set as follows: For given $\mathbf{c} \in \mathbb{R}^4$, find $v \in P_{4,mvp}(K)$ such that

$$\begin{aligned} (\nabla v, \nabla w)_K = 0, \quad & w \in P_{4,mvp,\mathbf{0}}(K), \\ v(\mathbf{m}_j) = c_j, \quad & j = 1,2,3,4. \end{aligned} \tag{3.7}$$

We denote the solution of the problem (3.7) by $v(\mathbf{c})$.

Now, We introduce a local finite element space. Let us set for $K \in \mathcal{T}_h$,

$$\mathcal{NC}_K^{OPT} = \{v(\mathbf{c}) \in P_{4,mvp,\mathbf{c}}(K) \mid \mathbf{c} \in \mathbb{R}^4\}.$$

The local degrees of freedom for $\mathcal{NC}_K^{OPT}$ are defined as follows

$$L_j(v) = \frac{1}{|e_j|} \int_{e_j} v d\sigma = v(\mathbf{m}_j), \qquad j = 1,2,3,4.$$

Since $P_{4,mvp}(K) = \mathcal{NC}_K^{DSSY} \oplus P_{4,mvp,\mathbf{0}}(K)$, the local finite element $\mathcal{NC}_K^{OPT}$ is obviously unisolvent. And we shall show that $P_1(K) \subset \mathcal{NC}_K^{OPT}$ in the next section. This means Bramble-Hilbert lemma holds for $\mathcal{NC}_K^{OPT}$.

Let $\mathcal{NC}_K$ be a nonconforming finite element satisfying $\mathcal{NC}_K \subset P_{4,mvp}(K)$ and $\dim(\mathcal{NC}_K) = 4$ with the same degrees of freedom as $\mathcal{NC}_K^{OPT}$. Let us define

nonconforming finite element spaces as follows

$$\mathcal{NC}_h^{OPT} = \{v_h \in L^2(\Omega) \mid v_h|_K \in \mathcal{NC}_K^{OPT} \text{ for } K \in \mathcal{T}_h, v_h \text{ is continuous at the midpoint of each } e \in \mathcal{E}_h\},$$

$$\mathcal{NC}_{h,0}^{OPT} = \{v_h \in \mathcal{NC}_{h,0}^{OPT} \mid v_h \text{ is zero at the midpoint of each } e \in \mathcal{E}_h \cap \partial\Omega\},$$

$$\mathcal{NC}_h = \{v_h \in L^2(\Omega) \mid v_h|_K \in \mathcal{NC}_K \text{ for } K \in \mathcal{T}_h, v_h \text{ is continuous at the midpoint of each } e \in \mathcal{E}_h\},$$

$$\mathcal{NC}_{h,0} = \{v_h \in \mathcal{NC}_h \mid v_h \text{ is zero at the midpoint of each } e \in \mathcal{E}_h \cap \partial\Omega\}.$$

As in [11], we can obtain the maximal inf-sup constant β^{OPT} such that $\beta \leq \beta^{OPT}$, where

$$\beta^{OPT} = \inf_{q \in P_{h,0}} \sup_{\mathbf{v} \in [\mathcal{NC}_{h,0}^{OPT}]^2} \frac{(\nabla_h \cdot \mathbf{v}, q)}{|\mathbf{v}|_{1,h}||q||_{0,\Omega}}, \quad \beta = \inf_{q \in P_{h,0}} \sup_{\mathbf{v} \in [\mathcal{NC}_{h,0}]^2} \frac{(\nabla_h \cdot \mathbf{v}, q)}{|\mathbf{v}|_{1,h}||q||_{0,\Omega}}.$$

The following theorem shows that $[\mathcal{NC}_{h,0}^{OPT}]^2$ has maximal inf-sup constant. The proof of the following theorem is almost same as theorem 2.2 in [11].

Theorem 3.3.3. *For inf-sup constants β^{OPT} and β corresponding to $\mathcal{NC}_{h,0}^{OPT}$ and $\mathcal{NC}_{h,0}$, respectively, an inequality $\beta \leq \beta^{OPT}$ holds.*

Proof. For any $q \in P_{h,0}$, let $\widehat{\mathbf{v}}(q) \in [\mathcal{NC}_{h,0}]^2$ satisfy

$$\frac{(\nabla_h \cdot \widehat{\mathbf{v}}(q), q)}{|\widehat{\mathbf{v}}(q)|_{1,h}||q||_{0,\Omega}} = \sup_{\mathbf{v} \in [\mathcal{NC}_{h,0}]^2} \frac{(\nabla_h \cdot \mathbf{v}, q)}{|\mathbf{v}|_{1,h}||q||_{0,\Omega}}. \tag{3.8}$$

Set $\mathbf{w}(q) \in [\mathcal{NC}_{h,0}^{OPT}]^2$ such that $\langle \mathbf{w}(q) - \widehat{\mathbf{v}}(q), 1 \rangle_e = 0$ for all $e \in \mathcal{E}_h$. Then we have $(\nabla_h \cdot \widehat{\mathbf{v}}(q), q)_K = (\nabla_h \cdot \mathbf{w}(q), q)_K$ for all $K \in \mathcal{T}_h$. Since $|\mathbf{w}(q)|_{1,h} \leq |\widehat{\mathbf{v}}(q)|_{1,h}$

from (3.6), using (3.8) we can see that

$$\begin{aligned}\sup_{\mathbf{v}\in[\mathcal{NC}_{h,0}]^2}\frac{(\nabla_h\cdot\mathbf{v},q)}{|\mathbf{v}|_{1,h}||q||_{0,\Omega}} &\le \frac{(\nabla_h\cdot\widehat{\mathbf{v}}(q),q)}{|\widehat{\mathbf{v}}(q)|_{1,h}||q||_{0,\Omega}}\\ \le \frac{(\nabla_h\cdot\mathbf{w}(q),q)}{|\mathbf{w}(q)|_{1,h}||q||_{0,\Omega}} &\le \sup_{\mathbf{v}\in[\mathcal{NC}_{h,0}^{OPT}]^2}\frac{(\nabla_h\cdot\mathbf{v},q)}{|\mathbf{v}|_{1,h}||q||_{0,\Omega}}.\end{aligned} \tag{3.9}$$

Let $\widehat{q}\in P_{h,0}$ satisfy

$$\sup_{\mathbf{v}\in[\mathcal{NC}_{h,0}^{OPT}]^2}\frac{(\nabla_h\cdot\mathbf{v},\widehat{q})}{|\mathbf{v}|_{1,h}||\widehat{q}||_{0,\Omega}} = \inf_{q\in P_{h,0}}\sup_{\mathbf{v}\in[\mathcal{NC}_{h,0}^{OPT}]^2}\frac{(\nabla_h\cdot\mathbf{v},q)}{|\mathbf{v}|_{1,h}||q||_{0,\Omega}}. \tag{3.10}$$

By using (3.9) and (3.10), we have

$$\begin{aligned}\beta = \inf_{q\in P_{h,0}}\sup_{\mathbf{v}\in[\mathcal{NC}_{h,0}]^2}\frac{(\nabla_h\cdot\mathbf{v},q)}{|\mathbf{v}|_{1,h}||q||_{0,\Omega}} &\le \sup_{\mathbf{v}\in[\mathcal{NC}_{h,0}]^2}\frac{(\nabla_h\cdot\mathbf{v},\widehat{q})}{|\mathbf{v}|_{1,h}||\widehat{q}||_{0,\Omega}}\\ \le \inf_{q\in P_{h,0}}\sup_{\mathbf{v}\in[\mathcal{NC}_{h,0}^{OPT}]^2}\frac{(\nabla_h\cdot\mathbf{v},q)}{|\mathbf{v}|_{1,h}||q||_{0,\Omega}} &= \beta^{OPT}.\end{aligned}$$

This completes the proof. □

Remark 3.3.4. *By choosing $\widetilde{c}$, the local basis function $\mu(x,y;\widetilde{c})$ of $\mathcal{NC}_K^{DSSY}$ can be determined as defined in [13]. We can get a hint of the reasonable choice of $\widetilde{c}$ from [11]. The way is to choose $\widetilde{c}$ such that the value of H_1-seminorm of the basis functions are minimum. This means that $\widetilde{c}$ can be found by solving the constrained minimization problem* (3.6) *by using $\Lambda(K) = \mathrm{Span}\{1,x,y,\mu_1(x,y),\mu_2(x,y)\}$ instead of $P_{4,mvp}(K)$, where $\mu_1(x,y)$, $\mu_2(x,y)$ are quartic polynomials such that $\mu(x,y;\widetilde{c}) = \mu_1(x,y) + \widetilde{c}\mu_2(x,y)$. Actually $\Lambda(K)$ is a subspace of $P_{4,mvp}(K)$ which has dimension 5. Since $\Lambda(K)$ has only one independent bubble function while $P_{4,mvp}(K)$ has 7 independent bubble functions, we may foresee that efficiency of the minimization problem for $\Lambda(K)$ is relatively worse than $P_{4,mvp}(K)$. $\mathcal{NC}_K^{OPT_1}$ and $\mathcal{NC}_h^{OPT_1}$ can be defined*

for $\Lambda(K)$ similarly to the definition of $\mathcal{NC}_K^{OPT}$ and $\mathcal{NC}_h^{OPT}$ for $P_{4,mvp}(K)$. The numerical results for $\mathcal{NC}_h^{OPT_1}$ will be presented in section 5.

3.4 Numerical scheme for basis functions

In this section, we present how to find local basis functions in each element K. Firstly, we need to find 11 basis functions of $P_{4,mvp}(K)$. However, since we know that $P_{4,mvp}(K) = \mathcal{NC}_K^{DSSY} \oplus P_{4,mvp,\mathbf{0}}(K)$ it is sufficient to find basis functions of $P_{4,mvp,\mathbf{0}}(K)$. This means that we have to solve a 8×15 linear system obtained from the mean value conditions and the vanishing conditions at midpoint of edges. By using the Gaussian-Jordan elimination, we can obtain 7 independent basis functions of $P_{4,mvp,\mathbf{0}}(K)$.

Let us denote 7 basis functions of $P_{4,mvp,\mathbf{0}}(K)$ by $\{q_j\}_{j=1}^7$. Let us denote by ϕ_1, ϕ_2, ϕ_3, and ϕ_4 1, x, y, and $\mu(x,y)$, respectively. Since $P_{4,mvp}(K) = \mathcal{NC}_K^{DSSY} \oplus P_{4,mvp,\mathbf{0}}(K)$, we can see that the basis of $P_{4,mvp}(K)$ is $\{q_k\}_{k=1}^7 \cup \{\phi_j\}_{j=1}^4$.

Now consider the constrained minimization problem. For given $\mathbf{c} \in \mathbb{R}^4$, find $v \in P_{4,mvp}(K)$ such that

$$\begin{aligned} (\nabla v, \nabla w)_K = 0, \quad & w \in P_{4,mvp,\mathbf{0}}(K), \\ v(\mathbf{m}_j) = c_j, \quad & j = 1,2,3,4. \end{aligned} \tag{3.11}$$

Let v be a unique solution of (3.11). Then, $v = \sum_{k=1}^7 \alpha_k q_k + \sum_{j=1}^4 \beta_j \phi_j$ for some constants α_k and β_j for $k = 1,..,7$ and $j = 1,..,4$. Since $\{q_j\}_{j=1}^7$ are bubble functions whose midpoint values are zero, there is no any contribution for conditions $v(\mathbf{m}_j) = c_j$ for $j = 1,2,3,4$. Thus $\beta_1, \beta_2, \beta_3$, and β_4 are uniquely determined by the second condition of (3.11). By using the first condition of

(3.11), we have

$$
\begin{aligned}
0 =&(\nabla v, \nabla q_l)_K \\
=&\sum_{k=1}^{7} \alpha_k (\nabla q_k, \nabla q_l)_K + \sum_{j=1}^{4} \beta_j (\nabla \phi_j, \nabla q_l)_K \\
=&\sum_{k=1}^{7} \alpha_k (\nabla q_k, \nabla q_l)_K + \beta_4 (\nabla \phi_4, \nabla q_l)_K - \sum_{j=1}^{3} \beta_j (\Delta \phi_j, q_l)_K + \sum_{j=1}^{3} \beta_j \left\langle \frac{\partial \phi_j}{\partial \nu}, q_l \right\rangle_{\partial K} \\
=&\sum_{k=1}^{7} \alpha_k (\nabla q_k, \nabla q_l)_K + \beta_4 (\nabla \phi_4, \nabla q_l)_K \qquad \text{for } l = 1, 2, ..., 7,
\end{aligned}
\tag{3.12}
$$

since $\Delta\phi_j$=0 on K and $\frac{\partial \phi_j}{\partial \nu}$ are piecewise constants for $j = 1, 2, 3$. Thus (3.12) gives the following 7×7 linear system

$$
(\nabla q_k, \nabla q_l)_K \gamma_k = -(\nabla \phi_4, \nabla q_l)_K, \qquad k, l = 1, ..., 7. \tag{3.13}
$$

We can find the coefficients α_ks by solving the linear system (3.13) and using that $\alpha_k = \gamma_k \beta_4$ for $k = 1, 2, ..., 7$. Since matrix $(\nabla q_k, \nabla q_l)$ is symmetric and positive definite, it is non-singular and the linear system (3.13) can be solved by iterative methods such as the conjugate gradient method. Thus we can determine all coefficients α_ks and β_js in this process.

Let $\mathcal{B} = \{\phi_1, \phi_2, \phi_3, \psi\}$ where $\psi = \sum_{k=1}^{7} \gamma_k q_k + \phi_4$ and γ_ks are determined by solving 7×7 linear system (3.13). Then clearly $\mathcal{NC}_K^{OPT} = \text{span}\mathcal{B}$. This means that Bramble-Hilbert lemma holds for $\mathcal{NC}_K^{OPT}$ because $P_1 \subset \mathcal{NC}_K^{OPT}$. If we look at more carefully the basis $\mathcal{B}$, then we can see that the basis $\mathcal{B}$ can be constructed by adding some bubble functions to the special basis function μ of the nonparametric DSSY element. Thus the process for finding basis functions of $\mathcal{NC}_K^{OPT}$ is to add the process of solving (3.13) to that of the

original nonparametric DSSY element.

The process of the construction for complete local basis functions of $\mathcal{NC}_K^{OPT}$ as follows.

(Step1) To find coefficients β_{jk} by solving the four 4×4 linear systems

$$\phi_k(\mathbf{m}_l)\beta_{jk} = \delta_{jl}, \quad l = 1, 2, 3, 4.$$

(Step2) To solve the 7×7 linear system (3.13) and obtain γ_l for $l = 1, 2, ..., 7$.

(Step3) To define basis functions $v_j = \sum_{k=1}^{3} \beta_{jk}\phi_k + \beta_{j4}\psi$ for $j = 1, 2, 3, 4$, where

$$\psi = \sum_{l=1}^{7} \gamma_l q_l + \phi_4.$$

Actually (Step1) is the same part for seeking local basis functions of $\mathcal{NC}_K^{DSSY}$. Thus the additional costs occur in (Step2). Surely it also costs to find 7 bubble functions $\{q_j\}_{j=1}^{7}$. However, as we shall see numerical results in the next section. it is not expensive at all to get speedup for computation.

3.5 Numerical results

In this section the proposed finite element $\mathcal{NC}_{h,0}^{OPT}$ and the nonparametric DSSY element $\mathcal{NC}_{h,0}^{np}$ are compared by numerical results for the two dimensional Stokes equations. In addition, numerical results for Remark 3.3.4 are presented.

Consider the following Stokes equations

$$\begin{aligned} -\Delta \mathbf{u} + \nabla p &= \mathbf{f} \qquad \text{in } \Omega, \\ \nabla \cdot \mathbf{u} &= 0 \qquad \text{in } \Omega, \\ \mathbf{u} &= 0 \qquad \text{on } \partial\Omega, \end{aligned}$$

which has the exact solution

$$\mathbf{u}(x,y) = \begin{pmatrix} e^{x+2y}(x^4 - 2x^3 + x^2)(2y^4 - 4y^2 + 2y) \\ -e^{x+2y}(x^4 + 2x^3 - 5x^2 + 2x)(y^4 - 2y^3 + y^2) \end{pmatrix},$$

$$p(x,y) = -sin(2\pi x)sin(2\pi y),$$

where $\Omega = (0,1)^2$. The triangulation of the domain Ω is given as shown in Figure 3.1 and the shape of the quadrilateral depends on the parameter $\theta \in (0,1]$.

We use the *Uzawa algorithm* to solve numerically the the above Stokes equations

$$(\nabla \mathbf{u}_h^{(n+1)}, \nabla \mathbf{v}) = (p_h^{(n)}, \nabla \cdot \mathbf{v}) + (\mathbf{f}, \mathbf{v}), \qquad \mathbf{v} \in [V_h]^2, \tag{3.14a}$$

$$(p_h^{(n+1)}, q) = (p_h^{(n)}, q) + \rho(\nabla \cdot \mathbf{u}^{(n+1)}, q), \qquad q \in P_{h,0}, \tag{3.14b}$$

where $\rho \in (0,1]$ and V_h is $\mathcal{NC}_{h,0}^{OPT}$ or $\mathcal{NC}_{h,0}^{np}$. Also the conjugate gradient method is used for solving elliptic problem (3.14a).

In Table 3.1, $\{\psi_j^{OPT}\}_{j=1}^4$ and $\{\psi_j^{DSSY}\}_{j=1}^4$ denote the local basis functions on K for $\mathcal{NC}_K^{OPT}$ and $\mathcal{NC}_K^{DSSY}$, respectively, such that $\psi_j^{OPT}(\mathbf{m}_k) = \delta_{kj}$ and $\psi_j^{DSSY}(\mathbf{m}_k) = \delta_{kj}$. As shown in Table 3.1, the ratio in energy norm between the two basis functions becomes smaller as parameter θ approaches 1. This means that the proposed finite element is more efficient than the

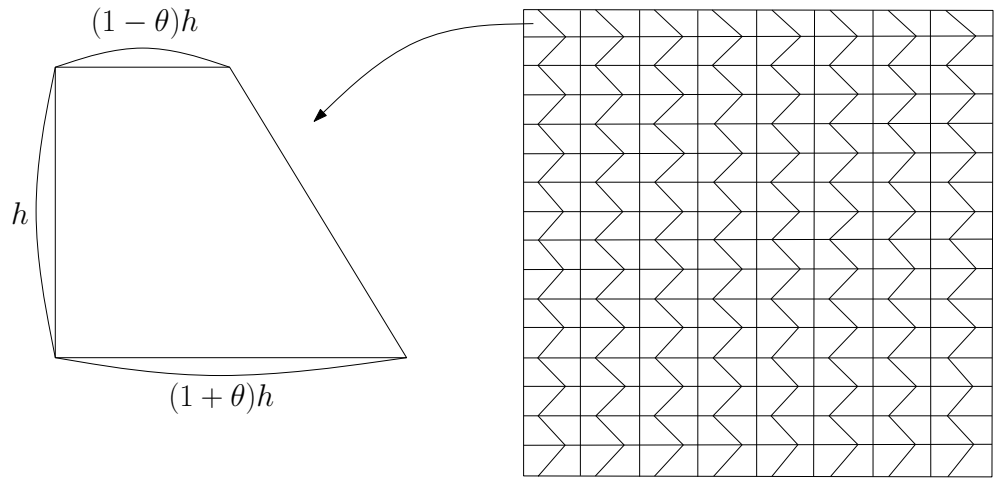

Figure 3.1: A quadrilateral triangulation and a quadrilateral with parameter $0 \leq \theta < 1$

nonparametric DSSY element as the quadrilateral gets closer to a triangle. Especially, when $\theta = 0$ the ratio is same.

In Table 3.2, the ratio of the computational time for OPT and DSSY elements are presented. We can see that the proposed finite element is more efficient than the nonparametric DSSY element in terms of the computational time. And as the shape of quadrilateral gets closer triangle the new finite element shows the better performance than DSSY element. Tables 3.3 – 3.8 present the approximation properties of numerical solutions and their optimal convergence properties. Two elements show similar results each other.

Tables 3.9 – 3.13 are the corresponding results to Tables 3.1 – 3.8 for OPT_1 and DSSY elements. As shown in Table 3.9, the ratio in energy norm between the two basis functions becomes smaller as parameter θ approaches 1. However, this is not as good as the case of OPT. Also $\widetilde{c}$ are presented in Table 3.9. This is a reasonable choice for $\widetilde{c}$ in the nonparametric DSSY element [13]. In Table 3.10, the ratios of the computational time for OPT_1 and DSSY elements show that OPT_1 is a little bit better than DSSY element

when θ is close to 1. But that is not as good as OPT in terms of computational time. Table 3.11, Table 3.12, and Table 3.13 shows that two elements have no differences in terms of the error of numerical solutions and convergence rate.

θ	0	0.3	0.5	0.7
R_1	1.0000	0.8742	0.6633	0.5142
R_2	1.0000	0.7588	0.6266	0.5126
R_3	1.0000	0.5823	0.4438	0.3517
R_4	1.0000	0.6093	0.4428	0.3565

Table 3.1: $R_j = |\psi_j^{OPT}|_{1,K}/|\psi_j^{DSSY}|_{1,K}$

h	$\theta = 0.3$	$\theta = 0.5$	$\theta = 0.7$
1/4	0.9286	1.0000	0.9594
1/8	0.9909	0.9409	0.9079
1/16	0.9722	0.9341	0.8680
1/32	0.9394	0.8942	0.8314
1/64	0.9145	0.8541	0.8109
1/128	0.8883	0.8377	0.7946

Table 3.2: Ratio of computing time t(OPT)/t(DSSY)

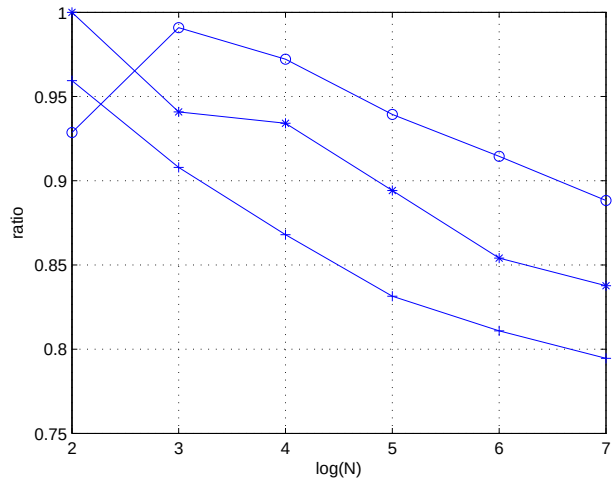

Figure 3.2: Ratio of computing time t(OPT)/t(DSSY). $*$, $\circ$, and $+$ implies $theta = 0.3$, $theta = 0.5$, and $theta = 0.7$ respectively.

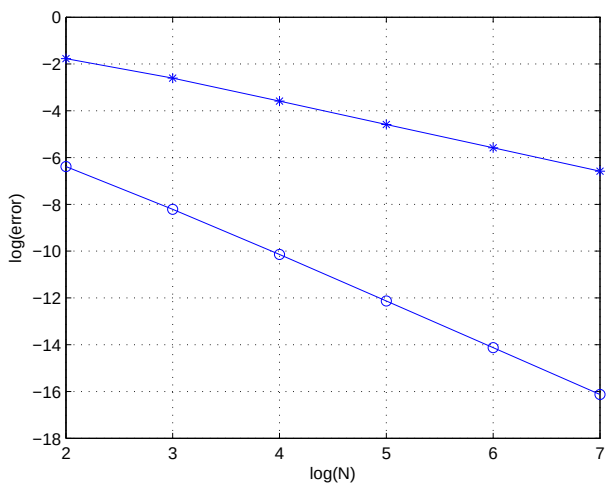

Figure 3.3: Comparison for results of OPT for the Stokes equations when $\theta = 0.3$. $*$ and $\circ$ implies $||p - p_h||_{0,\Omega}$ and $||\mathbf{u} - \mathbf{u}_h||_{0,\Omega}$, respectively.

h	$\|\|\mathbf{u}-\mathbf{u}_h\|\|_{0,\Omega}$	ratio	$\|\|p-p_h\|\|_{0,\Omega}$	ratio
1/4	0.1198e-01	-	0.2928	-
1/8	0.3371e-02	1.83	0.1644	0.83
1/16	0.8836e-03	1.93	0.8315e-01	0.98
1/32	0.2233e-03	1.98	0.4169e-01	1.00
1/64	0.5583e-04	2.00	0.2086e-01	1.00
1/128	0.1394e-04	2.00	0.1043e-01	1.00

Table 3.3: Comparison for results of OPT for the Stokes equations when $\theta = 0.3$.

h	$\|\|\mathbf{u}-\mathbf{u}_h\|\|_{0,\Omega}$	ratio	$\|\|p-p_h\|\|_{0,\Omega}$	ratio
1/4	0.1194e-01	-	0.2910	-
1/8	0.3483e-02	1.78	0.1637	0.83
1/16	0.9193e-03	1.92	0.8308e-01	0.98
1/32	0.2339e-03	1.97	0.4169e-01	0.99
1/64	0.5881e-04	1.99	0.2086e-01	1.00
1/128	0.1473e-04	2.00	0.1043e-01	1.00

Table 3.4: Comparison for results of the nonparametric DSSY elements for the Stokes equations when $\theta = 0.3$.

h	$\|\|\mathbf{u}-\mathbf{u}_h\|\|_{0,\Omega}$	ratio	$\|\|p-p_h\|\|_{0,\Omega}$	ratio
1/4	0.1210E-01	-	0.2841	-
1/8	0.4472E-02	1.44	0.1736	0.71
1/16	0.1236E-02	1.86	0.8833E-01	0.97
1/32	0.3197E-03	1.95	0.4439E-01	0.99
1/64	0.8090E-04	1.98	0.2223E-01	1.00
1/128	0.2032E-04	1.99	0.1112E-01	1.00

Table 3.5: Comparison for results of OPT for the Stokes equations when $\theta = 0.5$.

h	$\|\|\mathbf{u}-\mathbf{u}_h\|\|_{0,\Omega}$	ratio	$\|\|p-p_h\|\|_{0,\Omega}$	ratio
1/4	0.1262E-01	-	0.2852	-
1/8	0.4142E-02	1.61	0.1752	0.70
1/16	0.1151E-02	1.85	0.8849E-01	0.99
1/32	0.2988E-03	1.95	0.4439E-01	1.00
1/64	0.7556E-04	1.98	0.2223E-01	1.00
1/128	0.1895E-04	2.00	0.1112E-01	1.00

Table 3.6: Comparison for results of the nonparametric DSSY elements for the Stokes equations when $\theta = 0.5$.

h	$\|\|\mathbf{u}-\mathbf{u}_h\|\|_{0,\Omega}$	ratio	$\|\|p-p_h\|\|_{0,\Omega}$	ratio
1/4	0.1172E-01	-	0.2774	-
1/8	0.6098E-02	0.94	0.1866	0.57
1/16	0.1785E-02	1.77	0.9529E-01	0.97
1/32	0.4704E-03	1.92	0.4799E-01	0.99
1/64	0.1199E-03	1.97	0.2408E-01	0.99
1/128	0.3022E-04	1.99	0.1206E-01	1.00

Table 3.7: Comparison for results of OPT for the Stokes equations when $\theta = 0.7$.

h	$\|\|\mathbf{u}-\mathbf{u}_h\|\|_{0,\Omega}$	ratio	$\|\|p-p_h\|\|_{0,\Omega}$	ratio
1/4	0.1302E-01	-	0.2770	-
1/8	0.5424E-02	1.26	0.1898	0.55
1/16	0.1631E-02	1.73	0.9571E-01	0.99
1/32	0.4396E-03	1.89	0.4801E-01	1.00
1/64	0.1130E-03	1.96	0.2410E-01	0.99
1/128	0.2855E-04	1.98	0.1208E-01	1.00

Table 3.8: Comparison for results of the nonparametric DSSY elements for the Stokes equations when $\theta = 0.7$.

θ	0	0.3	0.5	0.7
R_1	1.0000	0.9667	0.8942	0.8183
R_2	1.0000	0.9743	0.9634	0.8949
R_3	1.0000	0.9743	0.9299	0.8825
R_4	1.0000	0.9482	0.8978	0.8576
$\widetilde{c}$	0.0000	0.1214	0.2239	0.2960

Table 3.9: $R_j = |\psi_j^{OPT_1}|_{1,K}/|\psi_j^{DSSY}|_{1,K}$ and $\widetilde{c}$

h	$\theta = 0.3$	$\theta = 0.5$	$\theta = 0.7$
1/4	1.7742	1.3684	0.9804
1/8	1.0319	1.0049	1.0093
1/16	1.0190	1.0041	1.0036
1/32	1.0122	1.0041	0.9953
1/64	1.0267	0.9984	0.9934
1/128	1.0200	0.9943	0.9915

Table 3.10: Ratio of computing time t(OPT_1)/t(DSSY)

h	$\|\|\mathbf{u} - \mathbf{u}_h\|\|_{0,\Omega}$	ratio	$\|\|p - p_h\|\|_{0,\Omega}$	ratio
1/4	0.1202E-01	-	0.2927	-
1/8	0.3368E-02	1.84	0.1644	0.83
1/16	0.8827E-03	1.93	0.8315e-01	0.98
1/32	0.2230e-03	1.98	0.4169e-01	1.00
1/64	0.5577e-04	2.00	0.2086e-01	1.00
1/128	0.1392e-04	2.00	0.1043e-01	1.00

Table 3.11: Computational results for OPT_1 for the Stokes equations when $\theta = 0.3$.

h	$\|\|\mathbf{u}-\mathbf{u}_h\|\|_{0,\Omega}$	ratio	$\|\|p-p_h\|\|_{0,\Omega}$	ratio
1/4	0.1273E-01	-	0.2852	-
1/8	0.4143E-02	1.62	0.1751	0.70
1/16	0.1150E-02	1.85	0.8849E-01	0.99
1/32	0.2984E-03	1.95	0.4439E-01	1.00
1/64	0.7544E-04	1.98	0.2223E-01	1.00
1/128	0.1892E-04	2.00	0.1112E-01	1.00

Table 3.12: Computational results for OPT_1 for the Stokes equations when $\theta = 0.5$.

h	$\|\|\mathbf{u}-\mathbf{u}_h\|\|_{0,\Omega}$	ratio	$\|\|p-p_h\|\|_{0,\Omega}$	ratio
1/4	0.1318E-01	-	0.2772	-
1/8	0.5449E-02	1.27	0.1897	0.55
1/16	0.1635E-02	1.74	0.9569E-01	0.98
1/32	0.4400E-03	1.89	0.4801E-01	0.99
1/64	0.1130E-03	1.96	0.2410E-01	0.99
1/128	0.2854E-04	1.99	0.1208E-01	1.00

Table 3.13: Computational results for OPT_1 for the Stokes equations when $\theta = 0.7$.

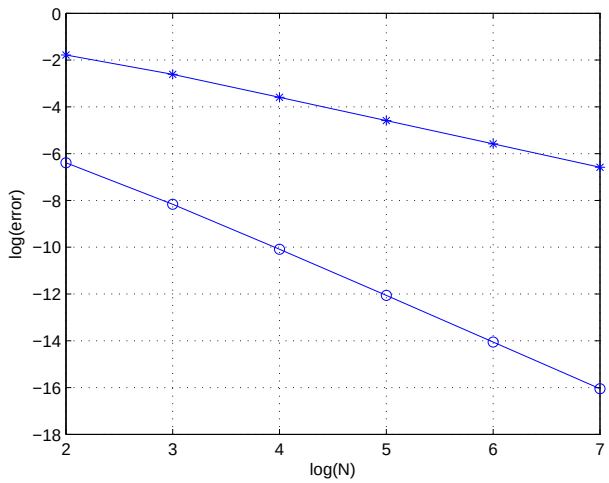

Figure 3.4: Comparison for results of the nonparametric DSSY elements for the Stokes equations when $\theta = 0.3$. $*$ and $\circ$ implies $||p - p_h||_{0,\Omega}$ and $||\mathbf{u} - \mathbf{u}_h||_{0,\Omega}$, respectively.

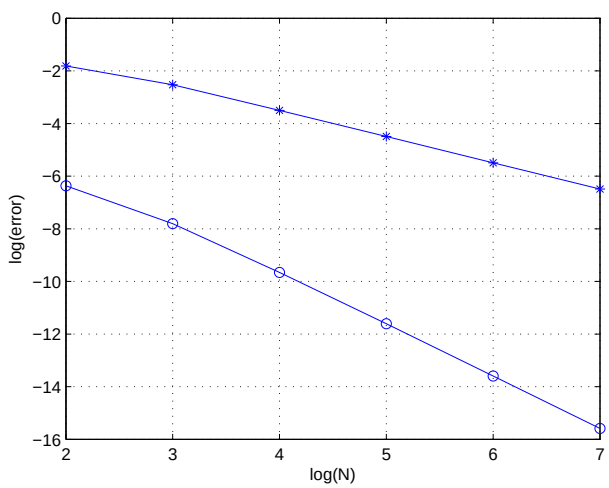

Figure 3.5: Comparison for results of OPT for the Stokes equations when $\theta = 0.5$. $*$ and $\circ$ implies $||p - p_h||_{0,\Omega}$ and $||\mathbf{u} - \mathbf{u}_h||_{0,\Omega}$, respectively.

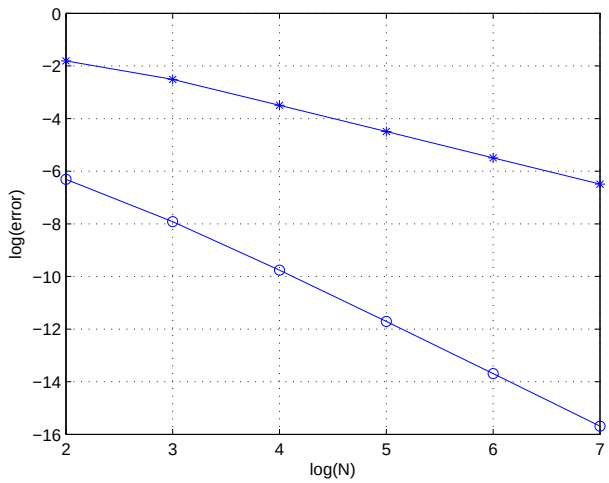

Figure 3.6: Comparison for results of the nonparametric DSSY elements for the Stokes equations when $\theta = 0.5$. $*$ and $\circ$ implies $||p - p_h||_{0,\Omega}$ and $||\mathbf{u} - \mathbf{u}_h||_{0,\Omega}$, respectively.

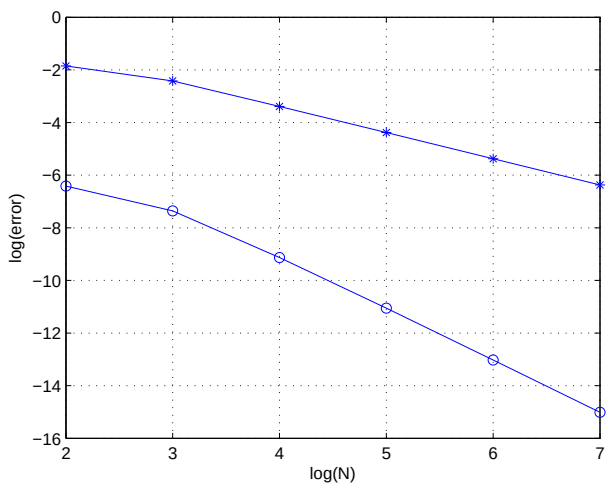

Figure 3.7: Comparison for results of OPT for the Stokes equations when $\theta = 0.7$. $*$ and $\circ$ implies $||p - p_h||_{0,\Omega}$ and $||\mathbf{u} - \mathbf{u}_h||_{0,\Omega}$, respectively.

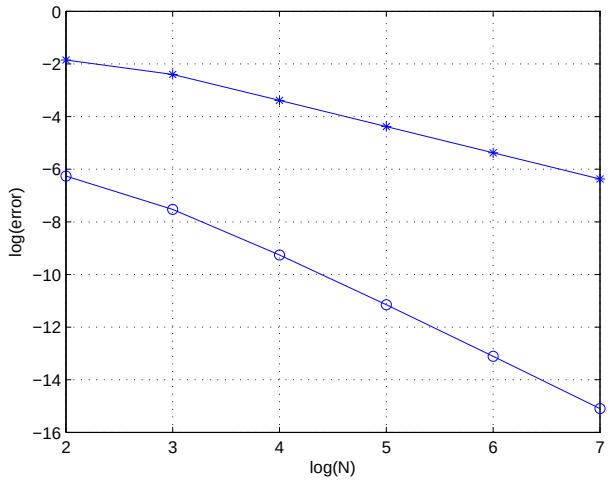

Figure 3.8: Comparison for results of the nonparametric DSSY elements for the Stokes equations when $\theta = 0.7$. $*$ and $\circ$ implies $||p - p_h||_{0,\Omega}$ and $||\mathbf{u} - \mathbf{u}_h||_{0,\Omega}$, respectively.

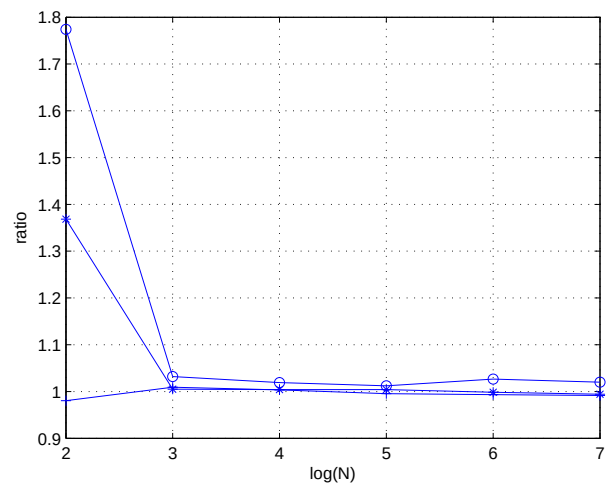

Figure 3.9: Ratio of computing time $t(OPT_1)/t(DSSY)$. $*$, $\circ$, and $+$ implies $\theta = 0.3$, $\theta = 0.5$, and $\theta = 0.7$ respectively.

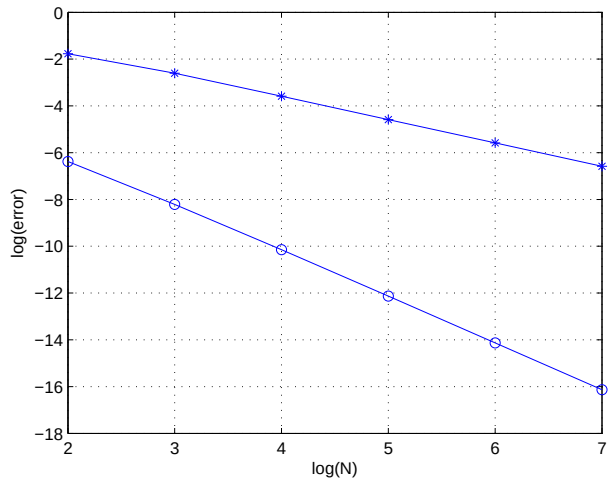

Figure 3.10: Comparison for results of OPT_1 for the Stokes equations when $\theta = 0.3$. $*$ and $\circ$ implies $||p - p_h||_{0,\Omega}$ and $||\mathbf{u} - \mathbf{u}_h||_{0,\Omega}$, respectively.

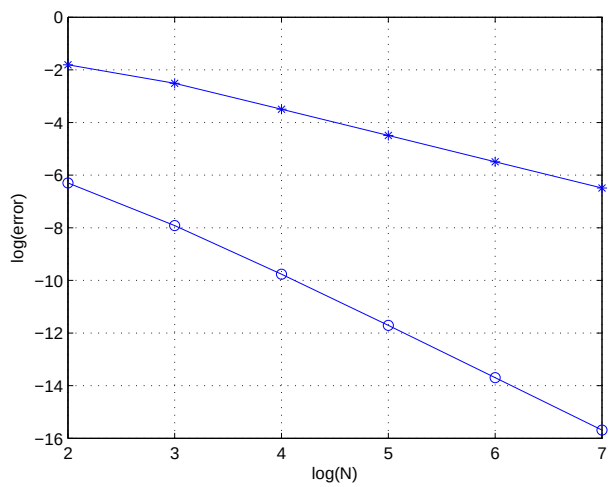

Figure 3.11: Comparison for results of OPT_1 for the Stokes equations when $\theta = 0.5$. $*$ and $\circ$ implies $||p - p_h||_{0,\Omega}$ and $||\mathbf{u} - \mathbf{u}_h||_{0,\Omega}$, respectively.

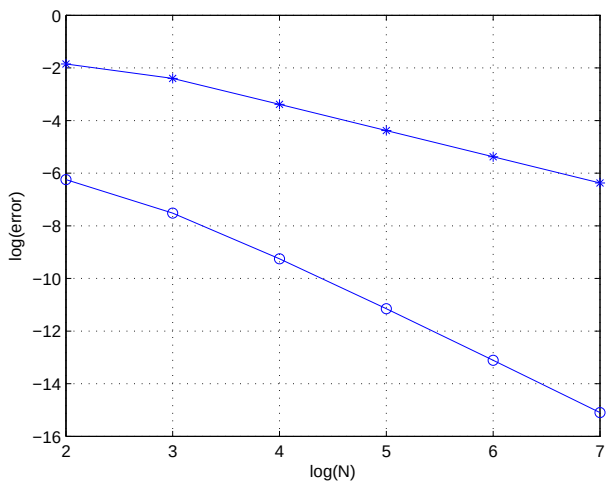

Figure 3.12: Comparison for results of OPT_1 for the Stokes equations when $\theta = 0.7$. $*$ and $\circ$ implies $||p - p_h||_{0,\Omega}$ and $||\mathbf{u} - \mathbf{u}_h||_{0,\Omega}$, respectively.

Bibliography

[1] D. N. Arnold, D. Boffi, and R. S. Falk. Approximation by quadrilateral finite elements,. *Math. Comp.*, 71:909–922, 2002.

[2] C. Bernardi, M. Dauge, Y. Maday, et al. Polynomials in the Sobolev world. 2007.

[3] S. C. Brenner and L. Y. Sung. Linear finite element methods for planar elasticity. *Math. Comp.*, 59:321–338, 1992.

[4] Z. Cai, J. Douglas, Jr., J. E. Santos, D. Sheen, and X. Ye. Nonconforming quadrilateral finite elements: A correction. *Calcolo*, 37(4):253–254, 2000.

[5] Z. Cai, J. Douglas, Jr., and X. Ye. A stable nonconforming quadrilateral finite element method for the stationary Stokes and Navier-Stokes equations. *Calcolo*, 36:215–232, 1999.

[6] Z. Chen. Projection finite element methods for semiconductor device equations. *Computers Math. Applic.*, 25:81–88, 1993.

[7] M. Crouzeix and P.-A. Raviart. Conforming and nonconforming finite element methods for solving the stationary Stokes equations. *R.A.I.R.O.–Math. Model. Anal. Numer.*, R-3:33–75, 1973.

[8] J. Douglas, Jr., J. E. Santos, D. Sheen, and X. Ye. Nonconforming Galerkin methods based on quadrilateral elements for second order elliptic problems. *ESAIM–Math. Model. Numer. Anal.*, 33(4):747–770, 1999.

[9] H. Han. Nonconforming elements in the mixed finite element method. *J. Comp. Math.*, 2:223–233, 1984.

[10] J. Hu and Z.-C. Shi. Constrained quadrilateral nonconforming rotated Q_1-element. *J. Comp. Math.*, 23:561–586, 2005.

[11] Y. Jeon, H. Nam, D. Sheen. A nonconforming quadrilateral element with maximal inf-sup constant. *Numer. Methods Partial Differential Equations*, 2013. in press.

[12] Y. Jeon, H. Nam, D. Sheen, and K. Shim. A nonparametric DSSY nonconforming quadrilateral element with maximal inf-sup constant. 2013. in preparation.

[13] Y. Jeon, H. Nam, D. Sheen, and K. Shim. A class of nonparametric DSSY nonconforming quadrilateral elements. *ESAIM–Math. Model. Numer. Anal.*, 2013. submitted (arXiv:1301.1120).

[14] M. Köster, A. Ouazzi, F. Schieweck, S. Turek, and P. Zajac. New robust nonconforming finite elements of higher order. *Applied Numerical Mathematics*, 62(3):166–184, 2012.

[15] R. Kouhia and R. Stenberg. A linear nonconforming finite element method for nearly incompressible elasticity and Stokes flow. *Comput. Methods Appl. Mech. Engrg.*, 124(3):195–212, 1995.

[16] C.-O. Lee, J. Lee, and D. Sheen. A locking-free nonconforming finite element method for planar elasticity. *Adv. Comput. Math.*, 19(1–3):277–291, 2003.

[17] P. Ming and Z.-C. Shi. Nonconforming rotated Q_1 element for Reissner-Mindlin plate. *Math. Models Methods Appl. Sci.*, 11(8):1311–1342, 2001.

[18] P. Ming and Z.-C. Shi. Two nonconforming quadrilateral elements for the Reissner–Mindlin plate. *Math. Models Methods Appl. Sci.*, 15(10):1503–1517, 2005.

[19] H. Nam, H. J. Choi, C. Park, and D. Sheen. A cheapest nonconforming rectangular finite element for the Stokes problem. *Comput. Methods Appl. Mech. Engrg.*, 257:77–86, 2013.

[20] C. Park and D. Sheen. P_1-nonconforming quadrilateral finite element methods for second-order elliptic problems. *SIAM J. Numer. Anal.*, 41(2):624–640, 2003.

[21] C. Park and D. Sheen. A quadrilateral Morley element for biharmonic equations. *Numer. Math.*, 2013. DOI 10.1007/s00211-013-0517-9.

[22] R. Rannacher and S. Turek. Simple nonconforming quadrilateral Stokes element. *Numer. Methods Partial Differential Equations*, 8:97–111, 1992.

[23] Z.-C. Shi. An explicit analysis of Stummel's patch test examples. *Int. J. Numer. Meth. Engrg.*, 20(7):1233–1246, 1984.

[24] Z. C. Shi. The FEM test for convergence of nonconforming finite elements. *Math. Comp.*, 49(180):391–405, 1987.

[25] S. Turek. *Efficient solvers for incompressible flow problems*, volume 6 of *Lecture Notes in Computational Science and Engineering*. Springer, Berlin, 1999.

[26] M. Wang. On the necessity and sufficiency of the patch test for convergence of nonconforming finite elements. *SIAM J. Numer. Anal.*, 39(2):363–384, 2001.

[27] Z. Zhang. Analysis of some quadrilateral nonconforming elements for incompressible elasticity. *SIAM J. Numer. Anal.*, 34(2):640–663, 1997.

국문초록

2차원에서 기존의 모수적 DSSY 유한요소는 평행사변형에서는 네개의 기저함수를 가지도록 정의하고 마주보는 변이 평행하지 않은 사각형에 대해서는 다섯개의 기저함수를 가지도록 정의해야만 최적의 수렴성을 보장할 수 있었다. 첫번째 장에서는 마주보는 변이 평행하지 않은 사각형에 대해서도 오직 네개의 기저함수를 가지도록 하는 비모수적 DSSY 유한요소를 소개한다.

두번째 장에서는 3차원에서의 모수적 DSSY 유한요소를 일반적인 육면체 격자로 확장하는 내용을 다룬다. 기존의 3차원에서의 모수적 DSSY 유한요소는 단지 평행육면체에서만 정의 되었다. 2차원에서와 같이 비모수적 방법을 이용하여 평행육면체 뿐만 아니라 일반적인 육면체에 대해서도 최적의 수렴성을 보장하는 새로운 유한요소를 소개한다.

마지막장에서는 스토크스문제를 효과적으로 풀기위한 유한요소로서 최대 inf-sup 상수를 가지는 비모수적 DSSY 유한요소를 소개한다. 이 유한요소는 각 사각형 요소에서 최소의 $H^1 - seminorm$를 갖도록 하는 최소화 문제를 접목하여 최대의 inf-sup 상수를 갖도록 하는 방법을 사용하여 정의한다. 이 유한요소는 첫번째장에서 소개한 비모수 DSSY 유한요소보다 계산시간 측면에서 우수하다는 것을 수치적 결과를 통해 보여준다.

주요어: 비순응 유한요소법, DSSY 유한요소, 비모수 유한요소, 비압축 스토크스 방정식, 타원형 편미분 방정식, 선형 탄성 문제

학번: 2010-30086

감사의 글

모두에게 감사합니다. 그리고, 제 아내에게 이 논문을 바칩니다.